Heritage Science

RESEARCH

Open Access

New dating approach based on the petrographical, mineralogical and chemical characterization of ancient lime mortar: case study of the archaeological site of Hippo, Annaba city, Algeria

Abderrahim Gheris[1*]

Abstract

This work presents the results of a multidisciplinary study on the characterization of the composition of certain joint mortars from the ancient city of *Hippo* (Algeria), one of the most important North African cities in antiquity. Twenty mortar samples were analysed by X-Ray Fluorescence (XRF), powder X-ray diffraction (XRPD), optical microscopy (OM), scanning electron microscopy (SEM) with energy dispersive X-ray analysis (EDS) and thermogravimetric analysis (TGA). Their main physical properties, like solid and dry density and porosity, have been measured by geotechnical procedures. The typological observation by OM showed the existence of four types of sand used as aggregates that ranged from fine to coarse and were mixed with a white to russet natural lime binder. These mortars consisted mainly of mixtures of calcite and rock fragments, and sometimes pieces of red tile. It was recognized that the origins of the natural granules were sands produced by marine erosion of the Edough Mountains. The analysis by XRPD and TGA indicates that the mortars consisted of a mixture of lime/aggregates of low to medium hydraulicity. The analysis of the main chemical components by XRF allowed for the confirmation of the dating of certain monuments and suggested a new dating for other monuments.

Keywords Petro physical analysis, Lime mortar, Aggregate, Roman ruin, *Hippo Regius*, Algeria

Introduction

Hippo, in Latin *Hippo Regius* and *Hippone* in French, is the ancient name of the city of Annaba, located in northeastern Algeria (Fig. 1). It became one of the main cities of Roman Africa. The name Annaba was chosen by the corsair *Kheireddine* (*Hayreddin Barbarossa*), who seized the city of the jujube (*El Annabe* in Arabic) in 1522 AD [1]. Prior to this, *Hippo* was "the gulf of the king, *Hippo Regius*", whose name goes back to prehistory following a subsidence in the crystalline mass of Mount Edough. The city sheltered a Phoenician settlement in the eleventh century BC. It was later a prosperous Punic city allied with Carthage, the then Numidian metropolis of King Massinissa, in the third century BC. The defeat of Juba I, an ally of Pompey, in 46 BC failed to entail its annexation to the Roman province of Africa Nova created by Julius Caesar. *Hippo* has known wealth and splendour. It was one of the largest cities of *Africa Nova* and the most opulent market in Roman Africa. In the fifth century AD, *Hippo* became the home of Christianity under the episcopate of St. Augustine, who

*Correspondence:
Abderrahim Gheris
a.ghris@univ-soukahras.dz
[1] Department of Civil Engineering, Faculty of Science and Technology, University of Souk Ahras, Route National 16, BP1553, 41000 Souk Ahras, Algeria

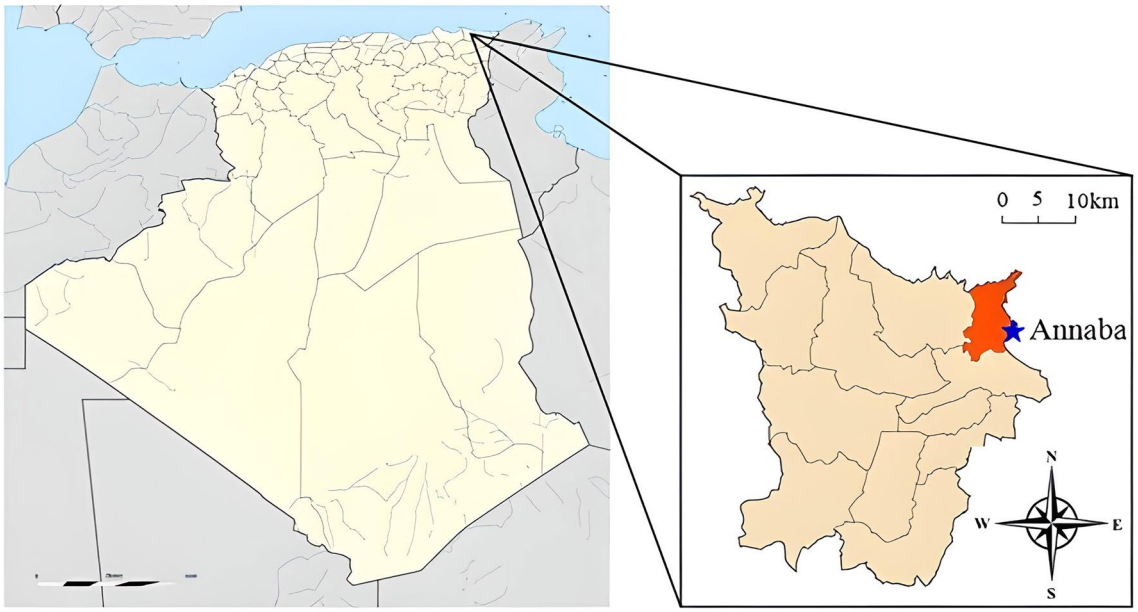

Fig. 1 Geographical location of Annaba city, *Hippo Regius* (King's gulf), the blue star designates the location of the ancient city of *Hippo Regius*

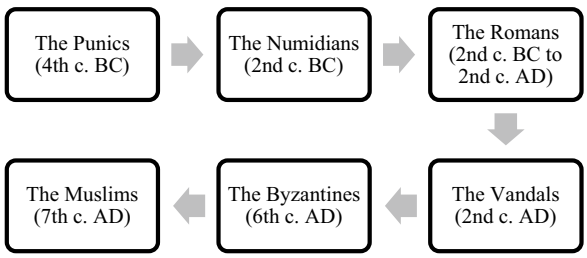

Fig. 2 Chronological progress of the indigenous cultures of *Hippo Regius* site

was bishop of the town from 396 AD until his death in 430 AD. *Hippo* was then taken by the Vandals in 431 AD and by the Byzantines in 533 AD. After long years of stagnation, *Hippo* fell under the thumb of Muslim dynasties in 705 AD, heralding the arrival of Islam. The ruins of *Hippo* are of great archaeological value, including the residential area from which most of the mosaics come, the Christian district where the *basilica* is located, the large baths and the forum. In the eleventh century, the *Sanhajas* built the town of *Madinat Zaoui* three kilometres away, which was occupied for a few years by the Spanish and French in the sixteenth century [2]. This city became more important than *Hippo* and was taken over by the French in 1832 AD and renamed Bone, before taking back its name of Annaba during the Algerian independence movement in 1962 AD, (Fig. 2).

Marec Erwan, director general of the excavations of *Hippo* during the colonial period, succeeded between 1947 and 1963 in the clearance of the historic city of *Hippo Regius* [3]. The archaeological site is composed of several insulae, each insulae has a particular function, from the main access to the site, we find [4]:

- The seafront villa district;
- The large *thermal baths* in the north;
- The Christian quarter;
  - The great *basilica.*
  - The outbuildings of the *basilica.*
  - The trefoil chapel.
- The *market* district;
- The *forum* quarter;
- The *Roman theatre.*

Most ancient Roman cities were built on a regular plan consisting of two main axes (*Cardo* and *Decumanus*) that divided the city into numerous small islands (*insulae*) and intersected in the city centre [2, 4]. But in the example of *Hippo*, we do not see this plan because the city was built by the Phoenicians and Romanized after the occupation of North Africa by the Roman Empire. Despite this, you can visualize: the two axes (*Cardo* and *Decumanus*) and the Roman buildings such as the great *basilica* and its annexes, the trefoil chapel, the villas on the seafront, as well as the forum

and the *market*; in a configuration closer to the regular Roman plan [2, 5].

Mortars are man-made lime materials that can provide valuable information on the constructive evolution of the building, on the provenance of the raw materials used for their production, and on the technological knowledge of ancient workers [6–19].

Physicochemical characterization of the old binders has been carried out previously prior to restoration work to allow the preparation of a binder of good compatibility with the original material [20]. Current restorers have been confronted several times with the question of hydraulic mortars: whether the lime itself is hydraulic or whether the materials contain pozzolanic compounds [21]. Most of the studies concerning this site have been devoted to its historical, urban and architectural aspects. For example, the historical dating of the *Hippo* ruins was carried out by Marec [5] on the basis of studies of mosaics and artefacts found during the first excavations between 1947 and 1963 [3]. Since then, no serious attempt has been made to confirm or refute the historical dating proposed by Marec [5]. In order to undertake the conservation and restoration of these ruins, a detailed knowledge of their structure and the basic natural materials used for their construction is necessary. Thus, the objective of this work is to determine the different granular portions that make up the joint mortar of the masonry, on the one hand and, on the other hand, to provide new detailed data on the petrographic, mineralogical and chemical composition of samples of mortars taken from *Hippo* (Fig. 3).

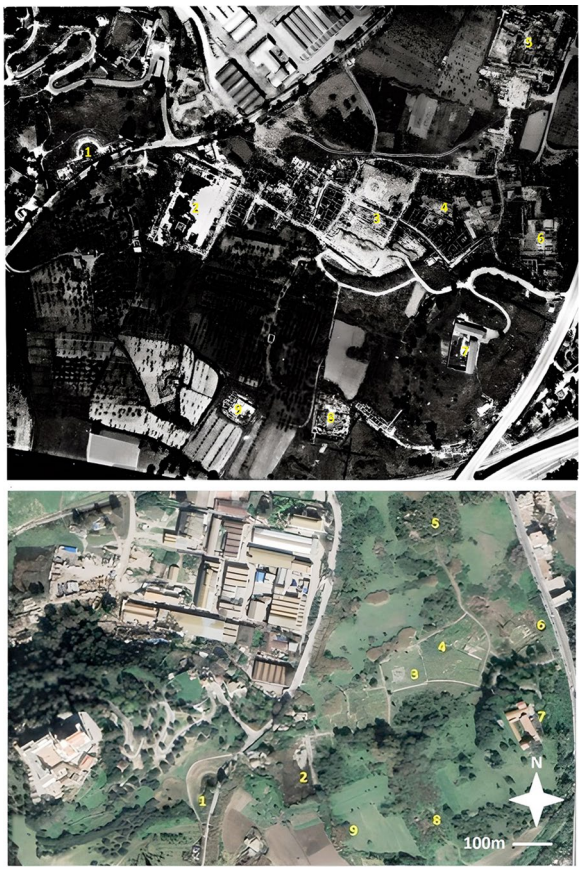

Fig. 3 The archaeological site of *Hippo*, greyscale picture: state of the excavations from Marec Erwan in 1963[3], colour picture: current status in 2022: **1**—Theatre, **2**—Forum, **3**—Market, **4**—Episcopal Quarter, **5**—Northern Baths, **6**—Sea-front villas, **7**—Museum, **8**—Southern Baths, **9**—Baths of the Minotaur

The invention of lime

Plaster renders were used in the walls of the city of *Çatalhöyük* in the sixth millennium BC, but it is in Egypt in the third millennium BC that one finds the use of plaster mortar to bind stones. For long centuries, the Orient utilized techniques based on plaster or lime, but it was not until the Hellenistic period that this technique was gradually introduced into Greek architecture. The Romans systematically used lime to make mortars for binding stone masonry, which allowed the application of concrete in their largest buildings [22]. The chemical reactions involved in the preparation of this latter lime, and in the setting of the mortar and in the carbonation of the binder, are:

(i) Preparation of quicklime by incineration of limestone between 900 and 1000 °C: $CaCO_3 \rightarrow CaO + CO_2$

(ii) Preparation of slaked lime (portlandite) by mixing quicklime with water: $CaO + H_2O \rightarrow Ca(OH)_2$ (portlandite) [23]

(iii) Carbonation of the binding phase: $Ca(OH)_2 + CO_2 \rightarrow CaCO_3 + H_2O$

The composition of Roman mortar

According to Vitruvius [24], the recipe for the preparation of mortars is as follows (Book II, Chapter 5): "*When the lime is extinguished, it must be mixed with the sand, in such proportion that there are three parts of cellar sand or two parts of river or sea sand, against one part of lime. This, indeed, is the fairest proportion of their mixture, which will be still much better if we add to the sand of the sea and the river a third part of poorly-fired crushed tiles. [Etiam in fluviatica aut marina si qui testam tunsam et succretam ex tertia parte adiecerit, efficiet materiae temperaturam ad usum meliorem]*". This is the first mention of the use of the red tile by Vitruvius "*testa or testam*" to improve the mortar. Furthermore, in Chapter 6 of Book II, he mentions pozzolana, the admirable volcanic powder that was used mainly near Vesuvius, which was added

to the mortar to harden it without exposure to CO_2 from the air. The pozzolan binder (one part lime and two parts powder) was used in the masonry of Romans port facilities. The question that arises is whether the Romans had knowledge of the properties of lime (hydraulic or air lime) that would explain the good performance of their works, even underwater (as hydraulic lime can harden underwater). The Romans must have made artificial hydraulic lime with either the *testa* or pozzolana, as Vitruvius specifically writes [24]. If not, how can the undeniable quality of many of their works be explained? With slaked lime "*Chaux grasse*, in French", buildings are not eternal, as Frizot [25] writes. The main compositions given by Vitruvius, as classified by Adam [23], are grouped in Table 1.

The *testa*, which Vitruvian translators translate as a tile or a poorly-fired tile, is a clay brick that has undergone cooking temperatures close to 600 °C and 700 °C [22]. The antique kilns used for firing bricks are identical to those used by potters, but the dimensions differ because of the large volume of materials that needed to be treated during each firing. It should be noted that in ceramic kilns, this temperature scale is not applicable for many materials. Indeed, these ovens cook between 800 °C and 900 °C to produce *terra sigillata* pottery and at around 1100 °C for other luxury products [22]. Such temperatures could be reached by ceramic kilns because the number of objects being fired was reduced. In the thesis by Frizot [26], he describes the high chemical efficiency of mixing the *testa* with lime to make mortars, but he fails to note that the pozzolanic chemical reaction is more easily achieved because the *testa* is made of kaolinic clay, which is a geological characteristic of Roman Italy and the majority of the Mediterranean countries. The pozzolanic reactions between lime and calcined clays have been studied for 50 years in several international laboratories. For example, Frizot [26] was able to say that between several types of calcined clays, only kaolinic clay gives good results after calcination between 650 and 800 °C. The other clays are less good, calcined illitic clays being mediocre or having no short-term effect. According to Frizot [26], the selection criterion is that of fast hardening, which allows the achievement of a compressive strength of 100 bar (10 MPa) at 28 days (according to the standard).

Table 1 The composition of the antique mortar according to Vitruvian, [23]

Binder	Aggregate	Water %
1 measure of lime	3 measures of quarry sand	15–20
1 measure of lime	2 measures of river or sea sand	15–20
1 measure of lime	2 measures of fluvial or marine sand + 1 measure of crushed *testa*	15–20
1 measure of lime	2 measures of pozzolan	15–20

Sampling and analytical techniques

In order to access the original mortar, the samples were taken by coring. Some samples could be recovered more easily thanks to the presence of exposed regions within the masonry.

Therefore, twenty joint mortars samples were sampled from the walls of *Hippo* (Fig. 4, Table 2). The names of the samples and their probable dating, based on the phases proposed by Marec [5], are shown in Table 2.

The chemical composition was obtained by X–ray fluorescence (XRF) using a Siemens *SRS3000/LARX10.* Portions of 6 g of pressed powders (maximum working pressure 25 bar) with a boric acid support were used to determine the chemical composition of the major elements (SiO_2, TiO_2, Al_2O_3, Fe_2O_3, MnO, MgO, CaO, Na_2O, K_2O and P_2O_5) [27]. The XRF results are shown in Table 3. Data reduction of the major elements was performed by the method proposed by Franzini et al. [28]. The measurement accuracy was ± 1% for SiO_2, TiO_2, Al_2O_3, Fe_2O_3, CaO, K_2O and MnO and ± 4% for MgO, Na_2O and P_2O_5. The detection limits are about 3 ppm to 3σ for most of the elements. The accuracy of trace elements is ± 2–3% at 1000 ppm; ± 5–10% at 100 ppm and ± 10–20% at 10 ppm. The weight loss for calcination (loss on ignition, L.O.I) was determined by calculating the loss in wt.% at 1100 °C, while the FeO content was determined by volumetric titration with $KMnO_4$ 10 N in an acidic solution.

According to the last column of Table 4, the hydraulicity index (Hi) values are reported for several samples. The hydraulicity index, i.e. the $(SiO_2 + Al_2O_3 + Fe_2O_3)/(CaO + MgO)$ ratio as defined by Vicat [29], was obtained by measuring the chemical compositions of several aggregate-free areas of approximately 20 × 20 μm^2 of mortar matrix (intergranular binder and lumps) through SEM/EDS.

To detect the elemental and mineralogical compositions of the binder samples, scanning electron microscope (SEM) and energy dispersive X-ray (EDS) techniques were applied on small sample fragments. EDS analysis was performed using a *Zeiss EVO/MA25* equipped with an secondary electron detector for microanalysis of the surfaces with a field emission cathode with a voltage of 20 kV (Research Unit for Iron and Steel Industry, Annaba, Algeria-RUISI). Wavelength dispersive microprobe analyses were performed with a *Zeiss EVO/MA25* instrument. For quantitative measurements, 15 kV acceleration voltage, 15 nA beam current on the Faraday cup, a defocused beam of 3.5 lm, and counting times between 15 s on the peak for Na, Mg, Al, Si, K, Ca, and Fe

Fig. 4 The site of study: **a** The ruins of *Hippo* and in the background the current *basilica* of Saint Augustine, **b** The *forum*, **c** The *marke*t, **d** The *Roman basilica*, **e** The *Roman theatre*, **f** Fountain of the mask of the *gorgon* and the *garum*, **g** The *Roman baths*

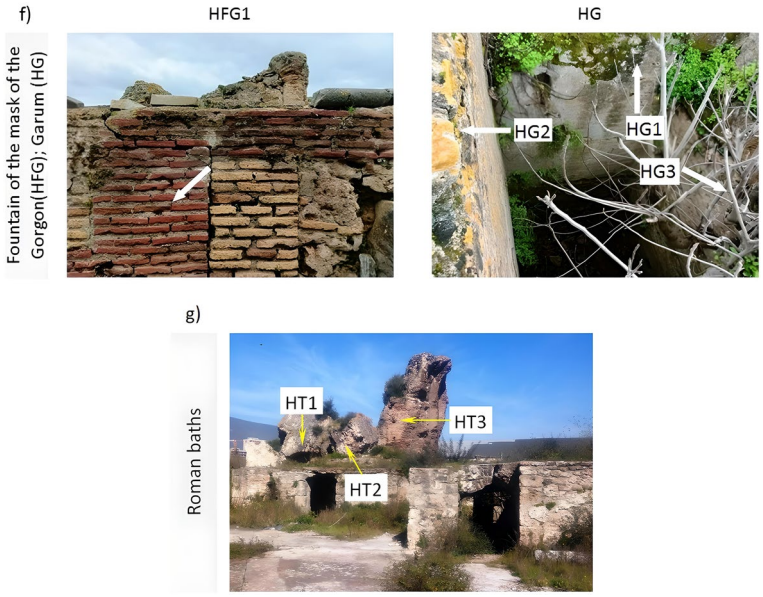

Fig. 4 continued

Table 2 List of joint mortar samples taken from *Hippo Regius* with location and probable dating based on historical studies

Sample code	Name of monument	Dating based on historical studies, AD [2, 5]	Sampling method
HFO1	Forum	1st c	Coring machine
HFO2	Forum	1st c	Coring machine
HFO3	Forum	1st c	Coring machine
HB1	Basilica	(?)	Manual
HB2	Basilica	(?)	Manual
HB3	Basilica	(?)	Manual
HFG1	Fountain of the mask of the Gorgon	End 2nd c	Coring machine
HG1	Garum[a]	(??)	Manual
HG2	Garum	(??)	Manual
HG3	Garum	(??)	Manual
HT1	Roman baths	3rd c	Manual
HT2	Roman baths	3rd c	Manual
HT3	Roman baths	3rd c	Manual
HT4	Roman baths	3rd c	Manual
HM1	Roman market	2nd c	Manual
HM2	Roman market	2nd c	Manual
HM3	Roman market	2nd c	Manual
HTR1	Roman theatre	2nd c	Coring machine
HTR2	Roman theater	2nd c	Coring machine
HTR3	Roman theater	2nd c	Coring machine

[a] *Garum*: from the Greek *garos* or *liquamen* in Latin [30], name given by the current archaeologists during the excavations of the fermentation tanks of a kind of fish sauce

(?) End 4th and early 5th c; (??) in progress of excavation

and 30 s for P, S, Ti, and Ba were chosen. Data processing was done with the smartSEM software, which is based on the U (qZ) correction method [31, 32]. The following standards were used for the analysis: Albite for Na, MgO (synthetic) for Mg, anorthite for Al, wollastonite for Si and Ca, sanidine for K, apatite for P, baryte for S, TiO_2

Table 3 Major elements concentration (in wt %) of the joint mortar samples obtained by XRF analysis

	SiO_2	Al_2O_3	Fe_2O_3	MnO	CaO	MgO	Na_2O	K_2O	TiO_2	P_2O_5	L.O.I	Sum
HFO1	38.22	1.23	1.18	0.04	45.21	1.12	1.45	0.83	0.16	0.50	10.06	100
HFO2	36.56	1.36	1.09	0.02	52.36	1.23	0.50	0.48	0.09	0.37	5.94	100
HFO3	40.02	1.41	1.13	0.02	47.20	1.02	0.84	0.42	0.03	0.11	7.80	100
HB1	42.83	1.51	0.43	0.01	47.84	1.17	0.09	0.13	0.05	bdl	5.94	100
HB2	41.32	1.85	0.38	0.01	51.78	2.02	0.08	0.15	0.07	bdl	2.34	100
HB3	43.57	1.27	0.40	0.02	49.02	2.48	0.05	0.17	bdl	bdl	3.02	100
HFG1	1.26	1.10	0.40	0.02	63.84	0.43	1.30	0.18	0.03	0.25	31.19	100
HG1	17.66	2.43	2.26	0.07	67.62	1.13	0.22	0.33	0.11	0.64	7.53	100
HG2	13.53	2.11	2.12	0.06	63.51	0.81	0.33	0.52	0.18	0.23	16.6	100
HG3	15.61	2.74	2.23	bdl	70.42	0.74	0.51	0.28	0.21	0.54	6.72	100
HT1	14.36	2.33	0.85	0.03	44.38	0.33	0.16	0.40	0.10	0.65	36.41	100
HT2	14.77	1.82	0.62	0.02	46.71	4.42	0.59	0.26	0.10	0.03	30.66	100
HT3	15.63	2.02	1.15	0.06	64.62	4.69	3.24	0.74	0.01	0.02	7.82	100
HT4	22.08	1.75	0.58	0.23	53.16	1.68	0.10	0.45	0.01	0.02	19.94	100
HM1	17.45	7.10	4.23	0.06	53.63	0.72	0.81	1.50	0.28	0.22	14.00	100
HM2	67.52	7.35	2.23	0.05	9.09	1.17	0.61	2.55	0.26	0.07	9.10	100
HM3	25.48	6.61	2.78	0.04	49.87	0.48	0.54	1.37	0.32	0.19	12.32	100
HTR1	47.46	3.89	2.43	0.02	42.48	1.01	0.42	0.54	0.34	bdl	1.41	100
HTR2	45.26	4.52	2.51	0.01	44.36	0.44	0.35	0.02	0.21	bdl	2.32	100
HTR3	42.87	2.42	2.74	bdl	46.41	1.42	0.51	bdl	0.18	bdl	3.45	100

Table 4 The chemical composition of the lime in the joint mortar samples performed by SEM–EDS microanalysis and Hydraulicity index (Hi)

	SiO_2	Al_2O_3	Fe_2O_3	CaO	MgO	Na_2O	ClO	K_2O	Sum	Hi
HFO1_L	19.32	0.49	0.20	74.67	1.27	3.32	0.31	0.42	100.00	0.26
HFO2_L	18.65	0.65	0.22	73.93	1.28	4.10	0.29	0.54	99.66	0.26
HFO3_L	20.28	0.51	0.22	73.70	1.25	3.28	0.32	0.44	100.00	0.28
HB1_L	14.23	0.60	bdl	82.36	1.35	0.23	0.09	1.14	100.00	0.18
HB2_L	8.03	0.59	0.10	80.69	10.11	0.20	bdl	0.28	100.00	0.10
HB3_L	13.88	0.62	0.20	79.88	4.01	0.22	0.09	1.10	100.00	0.18
HFG1_L	15.96	0.44	bdl	78.44	1.30	3.25	bdl	0.61	100.00	0.21
HG1_L	16.77	0.96	0.52	76.34	3.97	0.52	0.12	0.80	100.00	0.23
HG2_L	15.57	0.84	0.81	79.63	0.93	1.83	0.19	0.20	100.00	0.21
HG3_L	15.85	1.12	0.79	79.17	0.91	1.79	0.18	0.19	100.00	0.22
HT1_L	13.88	0.93	0.18	82.44	0.38	0.40	0.25	1.54	100.00	0.18
HT2_L	11.09	0.73	0.13	79.47	6.61	1.47	0.10	0.40	100.00	0.14
HT3_L	13.02	1.66	0.24	80.89	5.39	8.07	0.27	0.46	100.00	0.17
HT4_L	12.89	0.85	bdl	80.11	1.93	3.21	0.07	0.94	100.00	0.17
HM1_L	10.81	2.94	0.89	78.62	1.83	3.43	0.60	0.88	100.00	0.18
HM2_L	20.23	2.94	0.47	71.98	1.34	1.53	0.94	0.57	100.00	0.32
HM3_L	20.93	3.04	0.45	70.95	1.42	1.58	0.98	0.59	99.94	0.34
HTR1_L	15.06	2.13	0.11	82.32	0.28	bdl	0.10	bdl	100.00	0.21
HTR2_L	15.96	2.10	0.11	81.42	0.30	bdl	0.11	bdl	100.00	0.22
HTR3_L	16.95	1.51	0.12	80.95	0.34	bdl	0.13	bdl	100.00	0.23

bdl: below detection limit, $Hi = (SiO_2 + Al_2O_3 + Fe_2O_3)/(CaO + MgO)$

(synthetic) for Ti, rhodonite for Mn, haematite for Fe and celsian for Ba. Detection limits are calculated from the error propagation of the two measurements of the background signals of each X-ray line and are given as a 2—sigma value. The element distribution of Mg, Al, K, Ca, Fe (WDS) and S, Si (EDS) was mapped using an acceleration voltage of 15 kV and beam current of 30 nA. The acquisition time was set to 50 ms per step. The scan grid was spaced at 0.5 lm per step, covering in total 400 9 400 steps. Simultaneous acquisition of the backscatter signal in composition mode was performed.

The mineralogical analyses were carried out using a *ULTIMA IV Rigaku* diffractometer on the powders (powder fraction < 63 µm). The device was equipped with a scintillation detector (*X'Celerator Ultrarapide*), using Cu Kα radiation (λ Cu = 0.154056 nm), a nominal tube voltage of 40 kV and a current rating of 20 mA. The data were collected at 2θ = 7°–90°, in step of 0.02° 2θ with a step time of 2 s.

The *X'Pert HighScore Plus V3.0* software program (*PANalytical*) was used to identify the mineral phases in each X-ray powder diffractogram by comparing experimental peaks with *PDF − 2* database (International Centre for Diffraction Data (ICDD)).

Regarding thermal analysis, the prepared samples were heated from room temperature to 1000 °C at a rate of 25 °C/min. The thermobalance used in this study was the *Perkin Elmer Pyris* 1 *TGA* model. The heating environment (oven) was maintained in a nitrogen gas atmosphere with a flow rate of 15 ml/min. The oven was rapidly cooled with water from 1000 °C to 100 °C. A ceramic sample holder was used. The device was calibrated prior to beginning the tests, and the tests were performed in accordance with NF T 46-047 [33]. The Auto Step One software used with the analyser allows for high-resolution work and thus better distinguishes products that decompose in the same temperature range. In effect, when a large weight loss rate corresponding to the smaller peak is detected, (in this case a Step Rate of 0.100 mg/min was selected for the AutoStepOne scan), the heating rate is automatically reduced from the initial rate of 25 °C/min to that of the Step Rate (0.1 °C/min). The net result is that the *AutoStepOne* software inserts a slow scan step into the original program whenever the weight loss rate exceeds the Step On criterion. In this way, the *AutoStepOne* software generates a program with rapid heating rates in regions of little weight loss activity and slow heating rates or isothermal dwell times in regions of high weight loss activity.

The real density (γ_r) was measured using an automatic gas (He) pycnometer (*AccuPyc* II 1340, *Micromeritics Instrument Corporation*) on ~12 g of very fine-grained powders, (powder fraction < 63 µm) dried at 110 ± 5 °C for 24 h, according to ASTM D5550-06 [34–36]). Apparent density (γ_a) were performed on samples (~30 cm^3 by volume), according to ASTM D6683-19 [37]. The water total porosity was measured after water saturation following the standard recommended by the AFPC–AFREM [38], which consists of drying the samples at a temperature of 60 °C for 48 h until their mass becomes constant. After a degasification step under a primary vacuum for 24 h, the samples were submerged in water until they were saturated. The samples were weighed when dry, after saturation and in a hydrostatic condition. The total porosity, N_t, is calculated as:

$$N_t = \frac{M_2 - M_s}{M_2 - M_1} \times 100$$

where M_1 is the hydraulic weight of the sample, M_2 is the weight of the sample saturated with water and M_S is the weight of the dry sample.

The binder/aggregate ratio(B/A) expressed in wt.% was determined after mechanical disintegration and acid attack (HCl diluted, 1:5) of the samples [39]. Aggregate particle-size distribution was determined by sieving the sandy HCl-insoluble residue through sieves with 2, 1, 0.5, 0.250, 0.125 and 0.063 mm square openings.

Lastly, the statistical processing by exploratory analysis of the chemical and mineralogical data obtained by XRF and XRPD, was carried out by the "XLSTAT" software (v.2022) [40].

Results and discussion

Typology of the mortars

The observations of the main macroscopic features of the samples (colour of the binder, grain size of the aggregate, binder/aggregate ratio, and presence or absence of pieces of tiles) allowed us to identify four distinct groups (Table 3).

The M–I group (HG1–3, HFG1 and HM1) is characterized by slightly lower aggregate content and narrow grain size. The brownish-white type M-I mortar, called "fine mortar" (Fig. 5a), is poor in aggregates, with a lime/aggregate ratio of 1:0.5. The sand is made up of quartz and elements of metamorphic rocks, such as quartz gneiss. The grains are rounded and elongated.

The M–II group (HTR1–3, HB1–3 and HM2–3) is the most abundant mortar at the sampling site. It is a relatively gravelly mortar containing approximately 50% feldspathic sand. Its colour is pinkish white, with shades varying slightly between brown and greyish. Type M–II mortar (Fig. 5b) is a mortar with a lime to aggregate ratio of 1:1. The sandy fraction consists exclusively of crushed mica schist. The grains are angular, with diameters

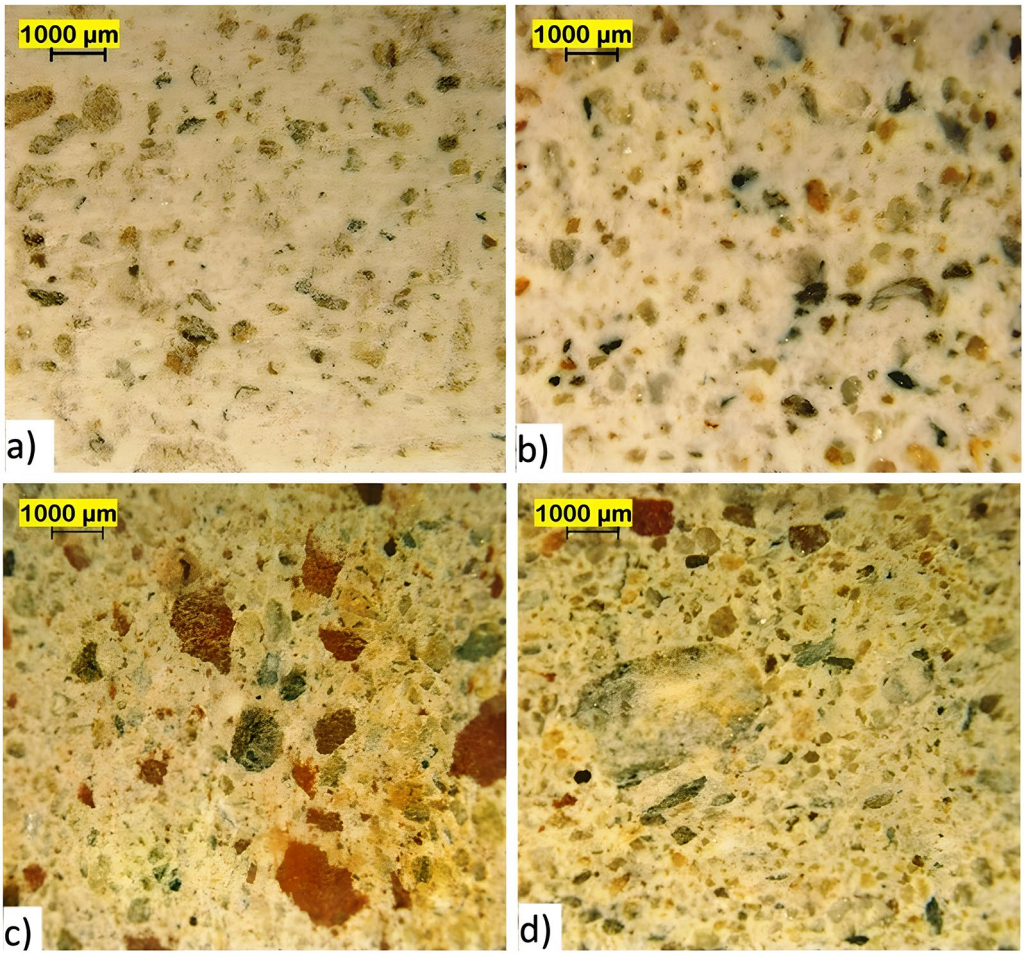

Fig. 5 Macrophoto under reflected light of mortars samples from different sectors of the ruins of *Hippo*. **a** Sample represents group M—I *garum*, **b** sample represents group M—II *market*, **c** Sample represents group M—III *Roman baths*, **d** Sample represents group M – IV *Roman theatre*

ranging from dust to 80 µm, with a large fraction less than 25 µm. The presence of a piece of crustacean shell in the mortar structure confirms the use of sea sand as aggregate.

The M–III group (HT1–4) appears very close to M–I, but is distinguished by its content of oxidized elements (presence of hematite) and the presence of tile fragments in its matrix. Reddish white mortar type M–III (Fig. 5c), referred to as "coarse mortar", had a lime to aggregate ratio of 1:2. The sand is made up of round grains of monocrystalline and polycrystalline quartz about 1 mm in diameter, associated with grains a few tens of micrometers in diameter of mica schists and feldspars, and sometimes plagioclase. The grain size range is wide; all dimensions are represented, ranging from a few micrometers to 10 mm. Some minerals, such as kaolinite and dickite, from clay groups have been highlighted by XRPD.

Finally, the M–IV type mortar (Fig. 5d) was a greyish white mortar with a lime to aggregate ratio of 1:3. The sand was composed of quartz and feldspar. The XRPD also indicated the presence of clay minerals. The grains are blunt to angular. Many grains had a diameter between 250 µm and 1 mm, but all dimensions between dust and 2 mm were present.

Chemical characterization

Figure 6a presents the results of the statistical analysis by agglomerative hierarchical clustering (AHC) performed on the different chemical elements obtained by XRF (see Table 3). This classification technique allowed us to identify three main groups according to the similarity of their chemical components [41]: Group 1 (HFO1–3, HFG1, HG1–3 and HT1), Group 2 (HB1–3 and HT2–4) and Group 3 (HM1–3 and HTR1–3). These groups represent a set of monuments that do not have the same age or time

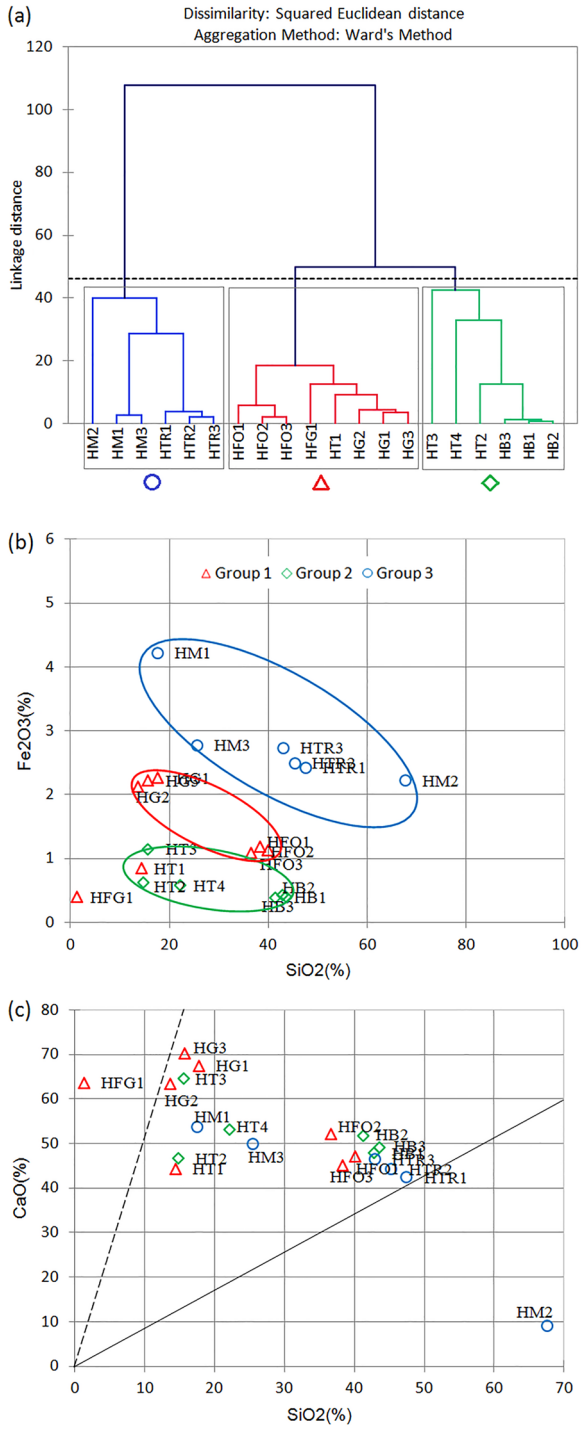

Fig. 6 **a** Dendrogram obtained by Agglomerative Hierarchical Clustering (AHC), using the results of analysis of the major chemical elements (except L.O.I). **b** Scatter plot, SiO_2 vs Fe_2O_3 (triangle and red ellipse: Group 1, rhombus and green ellipse: Group 2, circle and blue ellipse: Group 3). (**c**) Scatter plot SiO_2 vs CaO, black line represents a CaO/SiO_2 ratio; broken line represents 1: 0.187 ratio C/S; Solid line 1:1.16 C/S ratio

Table 5 Hydraulicity index and types of lime [42, 43]

Type of lime	Hydraulicity index (Hi)
Slaked lime (no hydraulic)	0–0.1
Low hydraulic	0.10–0.16
Medium hydraulic	0.16–0.30
hydraulic	0.30–0.40
Highly hydraulic	0.40–0.50

of construction. But we can estimate that the structures grouped in these three classes have the same components of aggregates (thus, the same mining origin) with, more or less, the same formulation of mortar. In addition, we can observe that the three groups obtained in the dendrogram (Fig. 6a) detached well. Figure 6b shows the scatter plot diagram Fe_2O_3 vs SiO_2 of the mortars, clustered according to the symbols and the groups identified by the AHC analysis. The fact that sample HT1 belongs to Group 1 instead of Group 2 initially led us to think that there was a measurement error due to contamination during the sampling operation. Therefore, we resumed the tests on other samples collected in the same place. The results obtained confirmed the first measurements. In our opinion, the fact that sample HT1 is detached from the family of HTs (thermal baths) is likely due to a change in the source of materials during the construction phase or a modification (or repair) that occurred later. In Fig. 6c, we can see that the majority of the samples have a CaO/SiO_2 ratio that varies from 1:1.16 (solid line) to 1:0.187 (broken line).

A hydraulicity index for the binder was calculated according to the Boynton [42] method as the ratio $(SiO_2+Al_2O_3+Fe_2O_3)/(CaO+MgO)$. The higher the index, the more hydraulic the properties of the mortar, Table 5 provides some benchmarks for estimating the hydraulicity content of lime.

If we compare the theoretical dates of the different monuments (second column of Table 6) with the groups obtained by AHC analysis (third column of Table 6), following the approach proposed by Miriello et al. [43], it can be seen that the construction phases of the different monuments are spread over two periods: from the first to the second century for the *forum*, the *market, and* the *Roman theatre;* and from the fourth to the fifth century for the *basilica* and the *Roman baths*. According to dating based on historical studies, the *Roman baths* were built in the middle of the third century. However, if we consider the time of construction of the *basilica*, a flagship monument of Christendom in this period that was

Table 6 Comparison between the theoretical dating of the constructions, and that obtained after analysis by the AHC classification technique

Samples	Probable dating based on historical studies [2, 5]	Groups obtained after AHC analysis (Fig. 6)[a]	Groups controlled by petrographic study and new proposal dating
HFO1	1st c	△	1st c
HFO2	1st c	△	1st c
HFO3	1st c	△	1st c
HB1	4–5th c	◇	4–5th c
HB2	4–5th c	◇	4–5th c
HB3	4–5th c	◇	4–5th c
HFG1	End 2th c	△	1st c
HG1	(?)	△	1st c
HG2	(?)	△	1st c
HG3	(?)	△	1st c
HT1	3rd c	△	4–5th c
HT2	3rd c	◇	4–5th c
HT3	3rd c	◇	4–5th c
HT4	3rd c	◇	4–5th c
HM1	2nd c	○	2nd c
HM2	2nd c	○	2nd c
HM3	2nd c	○	2nd c
HTR1	2nd c	○	2nd c
HTR2	2nd c	○	2nd c
HTR3	2nd c	○	2nd c

[a] In the third column, the symbols are that's of Fig. 6b, c

very well documented given its attachment with St. Augustine, we can estimate that the *Roman baths* were probably built in the middle of the fourth and the beginning of the fifth century. Alternatively, important restorations may have been carried out during the earlier period.

If we compare the theoretical dates of the different monuments (second column of Table 6) with the groups obtained by AHC analysis (third column of Table 6), following the approach proposed by Miriello et al. [43]. We can be seen that the construction phases of the different monuments are spread over two periods: from the first to the second century for the *forum*, the *market,* and the *Roman theatre;* and from the fourth to the fifth century for the *basilica* and the *Roman baths*. For the four samples (HT1–4) (Table 6, second and fourth column), it can be seen that there is no correspondence between the dating suggested by the historical studies and the results of the AHC analysis.

A possible explanation of this incongruence could be that these samples belong to several earlier and undocumented restoring operations. Indeed, the *Roman baths* were built during the reign of the Roman Emperor *Caracalla* between 211 and 217 AD (third century) [2]. However, if we consider the time of the construction of the *basilica* (the flagship monument of Christendom) which is very well documented, given its attachment to St. Augustine. As well as the existence on the site of the *basilica* of numerous burials date from the fourth century to the fifth century [2]. It can be said that the *basilica* actually dates from this period. So, we can estimate that the bases and the foundations of the *Roman baths* date from the third century, as for the upper parts, it dates from the fourth–fifth century.

From Table 6, we see that the *garum* that is currently in the excavation phase is classified in the first group, and so was probably built in the first century.

The Hi values in Table 4 allow us to classify the binders from Group 2 as weakly hydraulic mortars (Hi = 0.06–0.18), while those of Groups 1 and 3 are mostly moderately hydraulic mortars (Hi = 0.18–0.34).

The traditional lime preferred by ancient builders was nearly always air lime and was very pure. The rare examples of lime that was slightly or perfectly hydraulic were due to the poor quality of the limestone exploited

in the nearby geological environment. This agrees with the prescriptions given in the few texts that have come down to us, especially those of Vitruvian, which recommend the calcination of the hardest and whitest stones possible (*De Architectura*, Book VII, Chapter 2). However, the use of hydraulic mortars was common in antiquity, although in our case this hydraulicity was not supplied by the lime itself but by the aggregates used in its preparation.

Physical properties of the mortars

Table 7 shows the measured values of the main physical properties of the mortars analysed. The real densities (γ_r) of the samples vary from 2.40 to 2.62 g/cm^3, which are characteristic values of low-density binders. However, a mortar consisting of a carbonatic binder (calcite 2.71 g/cm^3) and a sandy aggregate (quartz 2.65 g/cm^3, plagioclase and feldspars 2.55–2.76 g/cm^3) should have a higher density than the analysed samples. The presence of low-density components, such as sea salt (2.1 g/cm^3 [44]), could explain these values. The other physical properties (Table 7), such as apparent density (γ_a) and the total porosity (N_t), depend mainly on the number of voids and present similar values for the samples from the *forum*, *basilica* and *Roman theatre*. In contrast, the samples from the *garum* and the *market* are more porous.

Table 7 Main physical properties of the samples, γ_r real density (g/cm^3), γ_a apparent density (g/cm^3), N_t porosity(%)

Sample	γ_r	γ_a	N_t
HFO1	2.61	1.90	27.20
HFO2	2.57	1.78	30.74
HFO3	2.62	1.91	27.10
HB1	2.61	1.91	26.82
HB2	2.57	1.88	26.85
HB3	2.60	1.90	26.92
HFG1	2.46	1.73	29.67
HG1	2.43	1.55	36.21
HG2	2.47	1.59	35.63
HG3	2.40	1.53	36.25
HT1	2.62	1.81	30.92
HT2	2.62	1.82	30.53
HT3	2.46	1.74	29.27
HT4	2.56	1.80	29.69
HM1	2.56	1.66	35.16
HM2	2.58	1.67	35.27
HM3	2.59	1.69	34.75
HTR1	2.58	1.80	30.23
HTR2	2.62	1.91	27.10
HTR3	2.62	1.92	26.72

Petrographic and mineralogical characterization of lime mortars

Mortar is a mixture of binder and aggregates of mineral origin. The mineralogical analysis by XPRD carried out on these mixtures showed that the mortars consisted mainly of quartz, feldspar, biotite, mica, plagioclase, and muscovite (Fig. 7a–g) and of clay minerals in smaller amounts.

The geological literature of the region of *Hippo Regius* (currently, the city of Annaba) suggests that the Edough Mountains are the probable origin of the minerals associated with these aggregates. These mountains consist of a set of metamorphic formations brought into contact tectonically, forming an antiform structure in the northeast to southwest direction [45]. According to an extract from the geological map of Mount Edough (Fig. 8), we observe the following layers. Migmatite (biotite gneisses and two-mica gneisses) [46], sometimes with benches of leptynites and marble, [47–49]. Above the gneisses is a region composed of garnet mica schists, kyanite, sillimanite and andalusite with benches of marble that are meters thick. A unit consisting mainly of sericoschist, chloritoschist and graphitic schist with centimetre- to meter-sized intercalations of quartzite caps the whole. The metamorphic complexes, as well as the sedimentary cover located mainly in the west of the massif, were intersected during the Miocene age by acidic magma, resulting in the generation of volcanic rocks [45].

Microscopic observations indicate that diatexites consist of phenoblasts (1–4 mm) of feldspars (plagioclase and orthoclase), quartz and micas (biotite and muscovite) (Fig. 9). Orthoclase predominates on plagioclase, and the crystals are often cracked and altered (Fig. 9a). Plagioclase appears in phenoblasts of variable size (2–5 mm) and albite macles (Fig. 9b). The micas form bands, more or less elongated, up to 1 cm. They alternate with quartzitic beds. Biotite is abundant, taking the form of brownish ribbons that are sometimes punctuated with opaque inclusions (iron oxides). The most altered biotite crystals have a corroded outline (Fig. 9c), as well as inclusions of ilmenite and rutile. Muscovite also occurs in sinuous beds and is sometimes found in porphyroclasts with a strongly altered and fragmented border (Fig. 9d) [45]. The presence of clay minerals was confirmed by XRD and was found to be mainly kaolinite (samples HT1–4).

Thermogravimetric analysis (TGA) was used as a tool for the characterization of ancient mortars. It can easily detect the presence of hydraulic compounds and provides information that allows the identification of the type of mortar. The weight loss percentage was estimated from the results of TGA as a function of temperature. The weight loss has different origins in different temperature ranges. Between 30 and 120 °C, the weight loss is due to

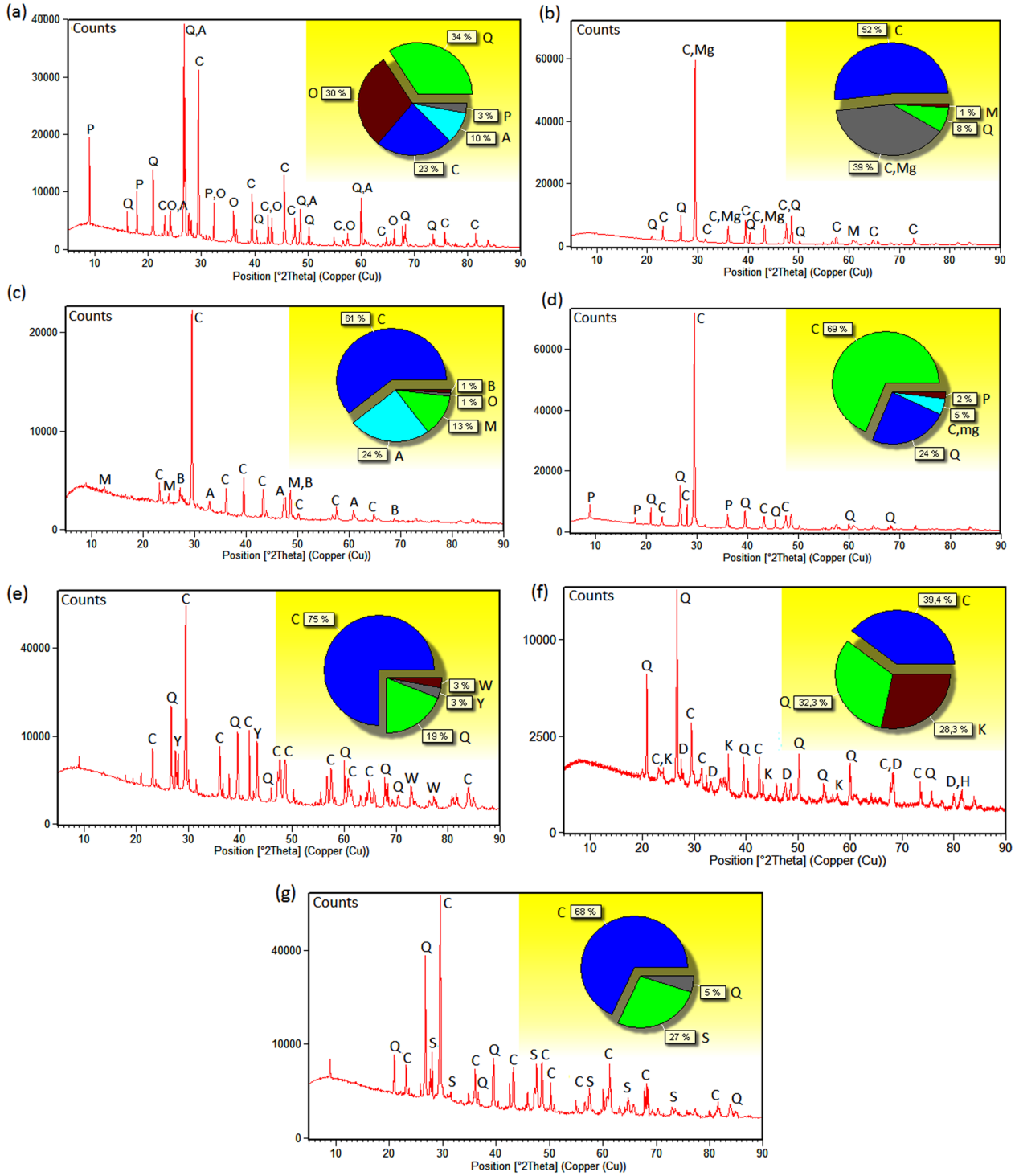

Fig. 7 Some typical examples of diffractograms of the samples: **a** HFO1; **b** HB2; **c** HFG1; **d** HG1; **e** HM1; **f** HT3; **g** HTR1. (Q: quartz; C: calcite; A: albite; B: biotite; O: orthoclase; P: polylithionite; M: muscovite; S: sepiolite; H: haematite; Y: yeelimite; K: kaolinite; D: dickite)

adsorbed water. From 120 to 200 °C, the weight loss of water comes from hydrated salts. From 200 to 600 °C, the loss of weight is due to structurally bound water, SBW. Finally, between 600 and 800 °C, the loss of CO_2 is due to the decomposition of calcium carbonate ([50–52]). In hydraulic mortars, the SBW is greater than 3%, and in

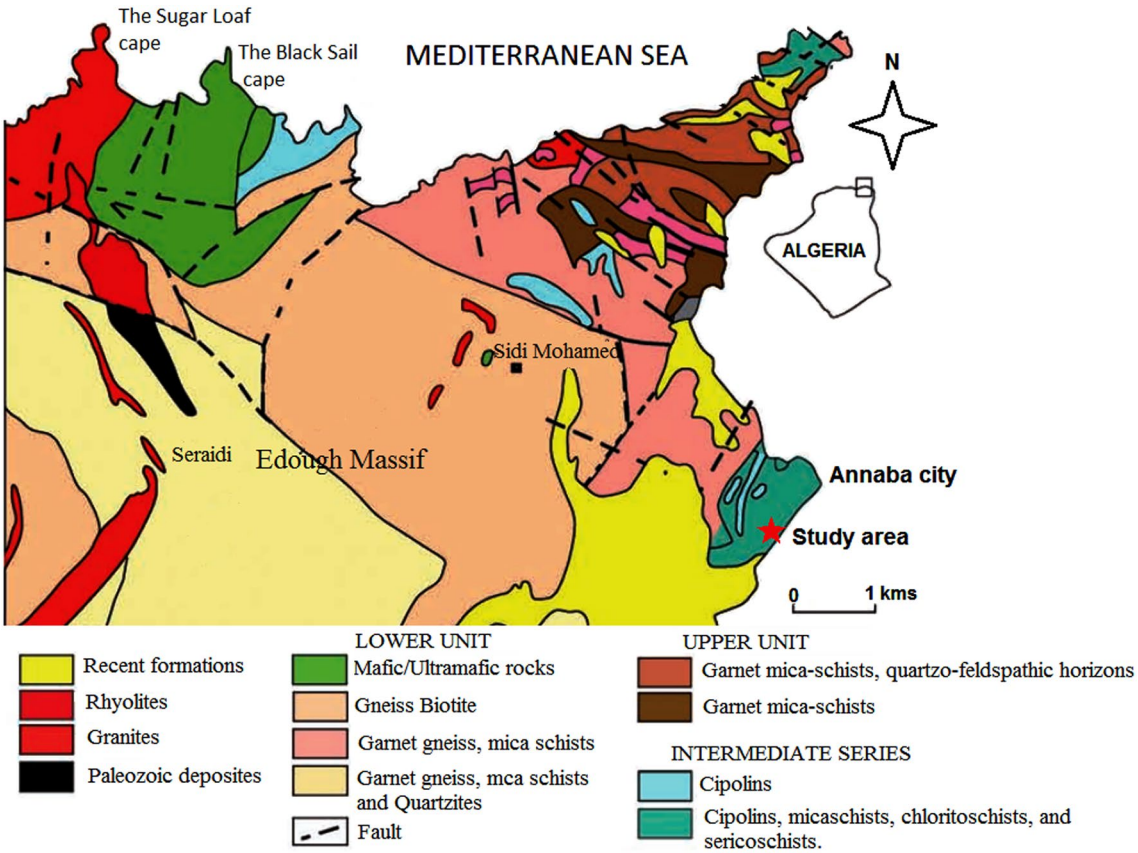

Fig. 8 Simplified geological maps of the Edough Massif (modified on the basis of works of [47–49])

non-hydraulic mortars (i.e. typical lime mortars, Fig. 10a the value is less than 3% (and the CO_2 loss over 600 ∘C is greater than 32%) [53–55]. If the CO_2/H_2O ratio is less than 10, the hydraulic character can be affirmed [20, 56]. A mortar sample could be classified as strongly hydraulic if, after analysis of the CO_2/SBW vs CO_2 binary diagram, the CO_2/SBW ratio is less than 5 and the CO_2 is less than 15% [57]. If the ranges are 15–25% for CO_2 and 5–10 for the CO_2/SBW ratio, the compounds can be classified as hydraulic or artificial pozzolanic mortars [54, 56–58]. These data are shown in Fig. 10 and Table 8.

From the CO_2/SBW vs CO_2 binary diagram (Fig. 10b), it can be deduced that none of the tested samples meet the requirements for hydraulic or man-made pozzolanic materials. Since the CO_2/SBW ratios are less than 10, the hydraulicity can also be assumed for ten samples (HTR1–3, HG1–3, HFO1–3 and HM2).

In order to distinguish the lime fraction from the aggregates, one must determine the % total weight loss once the calcium carbonate ($CaCO_3$) has decomposed. That is to say, the initial weight of the sample (100%), minus the % weight loss obtained in the temperature range 600–800 °C. The samples (HTR2, HG1–3, HM3, HFO3 and HFG1) have a % total weight loss once the carbonate has decomposed in the order of 73% average. This corroborates the XRPD results: lower quantity of quartz in these binders, and therefore a higher percentage of calcite.

The hydraulic mortar has the property of hardening when water is added to the dry binder, and also has the ability to harden underwater. The hydraulic compounds (C–S–H, Calcium Silicate Hydrate) are obtained from the reaction of certain minerals with portlandite ($Ca(OH)_2$) [59]. Thermogravimetric data on the tested binders revealed H_2O and CO_2 contents ranging from 2.04 wt.% (HT2) to 3.63 wt.% (HTR1) for H_2O and 27.76 wt.% (HM2) to 33.99 wt.% (HB1) for CO_2. Therefore, CO_2/H_2O ratios from 7.86 (HTR1) to 16.62 (HT2) were obtained.

In Fig. 11, the distribution of the main different elements of minerals composing of the mortars is shown in the ternary diagram, where the modal percentages of quartz (Qds, sand presence indicator), calcite ($CaCO_3$, for the proportion and type of the binder) and rock fragments (Rf, proportion remaining by subtracting

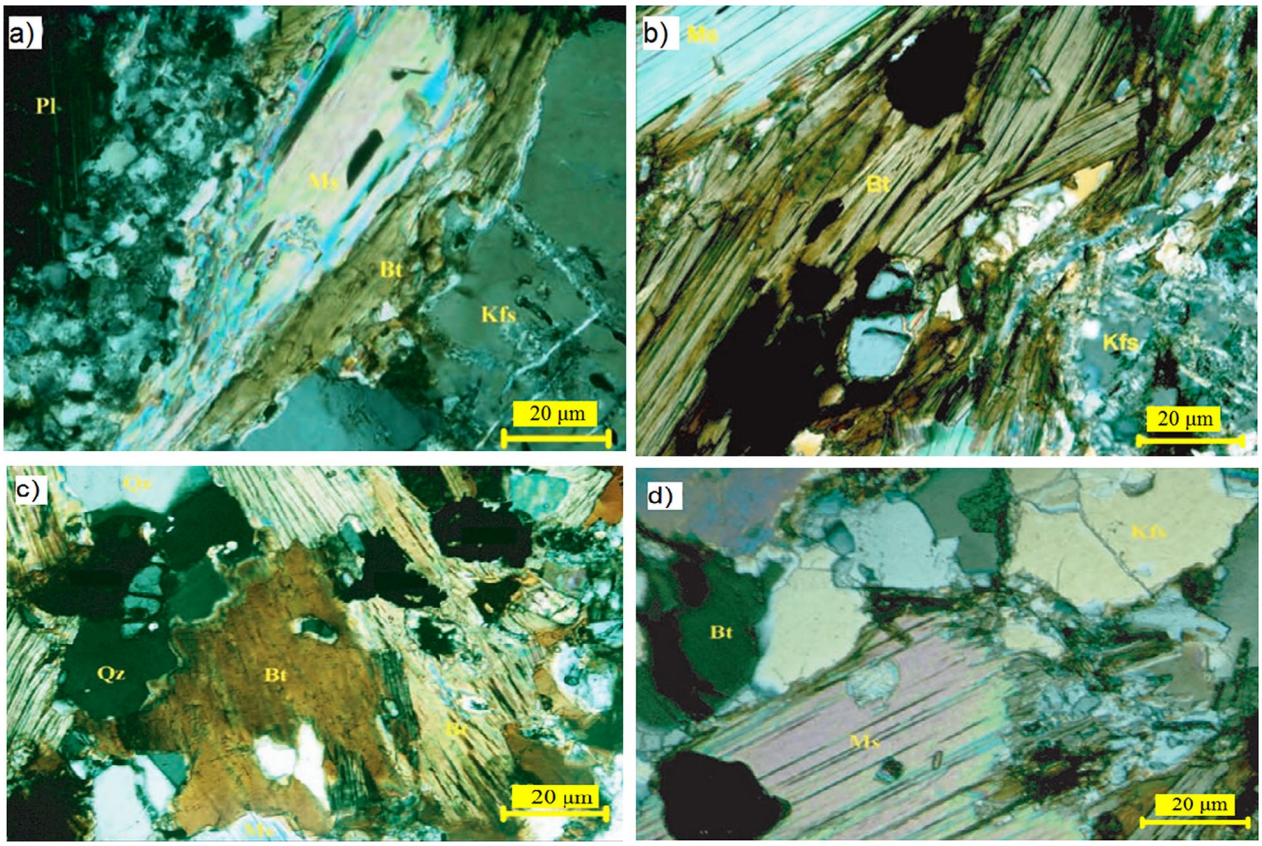

Fig. 9 Thin section micrographs by polarised light microscopy according to Hadj Zobir [45]; **a** porphyroblast diatexites of altered feldspars; **b** In this thin blade, the alteration of the potassic feldspars is more extensive; **c** Biotite strongly altered and corroded; **d** Altered Muscovite. Bt: biotite, Kfs: potassic feldspar, Ms: muscovite, Qz: quartz, Pl: plagioclase

quartz and calcite) have been reported. Calcite, a mineral indicative of the presence of lime, was detected in almost all samples with very variable proportions, from 22% (HFO2) to 85% (HFG1). Quartz, or silicon oxide, was relatively present in the mortars from the construction of the *baths* (HT1–4) and the *market* (HM1–3) but was less present in the *basilica* and the *garum*. As for the remaining components (rock fragments), there was a weak presence at the *garum* (HG1–3) and the *market* (HM1–3), and average values for the rest of the monuments.

In mineralogy, we often a get large multivariate datasets, for example consisting of thousands of data points in the form of peaks of the diffractograms [60]. In order to better visualize the information contained in these diffractograms, data mining was carried out using a statistical technique called principal component analysis (PCA). Principal components analysis (PCA) is probably the most widely used and best known chemometric (or indeed multivariate) technique [61]. In the world of PCA, information is called inertia and dimensions are called factors or axes. In order to take advantage of PCA analysis, we organized our different samples (20 samples or observations) according to six quantitative variables. Bringing together both the mineralogical properties represented by the rate of precedence of quartz (in %), calcite (in %), and finally the rock fragments (in %) (see Table 8, Fig. 7). As well as the physical characteristics of the mortar such as: porosity (in %), apparent density (in g/m^3) and the binder/aggregate ratio (in %) (see Table 9 and Table 7). In the principal component analysis, variables are often preprocessed. This is particularly recommended when the variables are measured in different units (for example: g/m^3, kilograms, %, …) or when the variables have different orders of magnitude. In our study, we used a technique called standard normalization, also called z-score normalization [62]. This method commonly used in the principal component analysis or in the machine learning algorithms. Technically, the approach consists of transforming the raw data by subtracting from each variable a reference value (the mean of the variable) and dividing it by the standard deviation. At the end of this transformation, the data obtained are

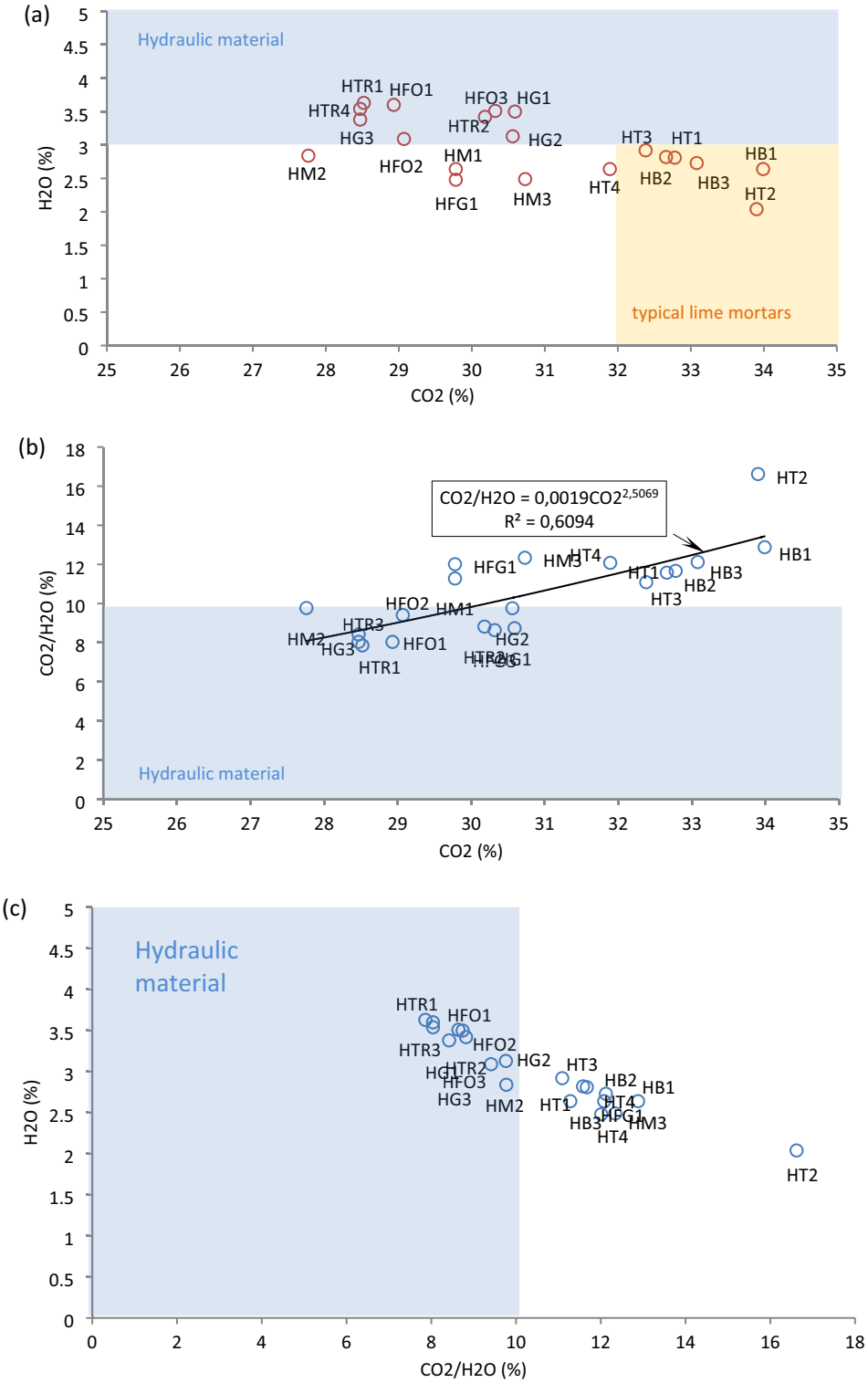

Fig. 10 Thermal analysis: **a** structurally bound water, SBW (H_2O weight loss % within the range 200–600 °C) vs. carbonate decomposition (CO_2—weight loss % above 600 °C); **b** binary diagram of CO_2/SBW vs. CO_2; (**c**) structurally bound water vs. CO_2/SBW ratio

Table 8 Thermogravimetry and XRPD results on all samples, (powder fraction < 63 µm)

Sample	Mass loss per temperature range (°C)							XRPD results[a]		
	< 120 (%)	120–200 (%)	200–600 (%)	> 600 (%)	H_2O (%)	CO_2 (%)	CO_2/H_2O (%)	Calcite (%)	Quartz (%)	Rf (%)
HTR1	1.31	0.59	3.69	24.12	3.63	28.52	07.86	34.00	23.00	43.00
HTR2	1.23	0.57	3.04	26.24	3.42	30.18	08.82	31.00	22.00	47.00
HTR3	1.31	0.60	3.39	23.94	3.54	28.47	08.04	35.00	23.00	42.00
HB1	2.31	0.40	2.86	20.94	2.64	33.99	12.88	10.00	49.00	41.00
HB2	2.29	0.49	2.80	19.47	2.81	32.78	11.67	8.00	52.00	40.00
HB3	2.31	0.39	2.83	20.12	2.73	33.08	12.12	9.00	50.00	41.00
HFG1	2.20	0.57	3.11	27.12	2.48	29.78	12.01	0.00	85.00	15.00
HG1	1.21	0.47	3.25	26.77	3.50	30.59	08.74	24.00	69.00	7.00
HG2	1.24	0.48	3.10	26.06	3.13	30.56	09.76	5.00	79.00	16.00
HG3	1.20	0.57	3.02	27.12	3.38	28.47	08.42	6.00	70.00	24.00
HM1	2.75	0.90	2.95	23.94	2.64	29.78	11.28	28.00	38.00	34.00
HM2	2.88	1.06	3.25	23.77	2.84	27.76	09.77	30.50	43.00	26.50
HM3	2.81	1.01	3.10	26.94	2.49	30.73	12.34	35.00	38.00	27.00
HFO1	2.99	0.89	2.91	24.65	3.60	28.93	08.04	32.30	39.40	28.30
HFO2	3.08	0.79	3.03	24.83	3.09	29.07	09.41	19.00	75.00	6.00
HFO3	3.23	0.57	3.08	26.41	3.51	30.32	08.64	25.00	64.00	11.00
HT1	1.30	0.49	1.66	18.30	2.82	32.66	11.58	23.00	66.00	11.00
HT2	1.24	0.58	1.91	19.89	2.04	33.90	16.62	10.00	45.00	45.00
HT3	1.31	0.60	2.72	20.94	2.92	32.38	11.09	8.00	48.00	44.00
HT4	1.32	0.60	2.84	18.77	2.64	31.89	12.08	9.00	42.00	49.00

[a] As indicated by the intensity of XRPD peaks (see, Fig. 7). Rf: Rock fragments

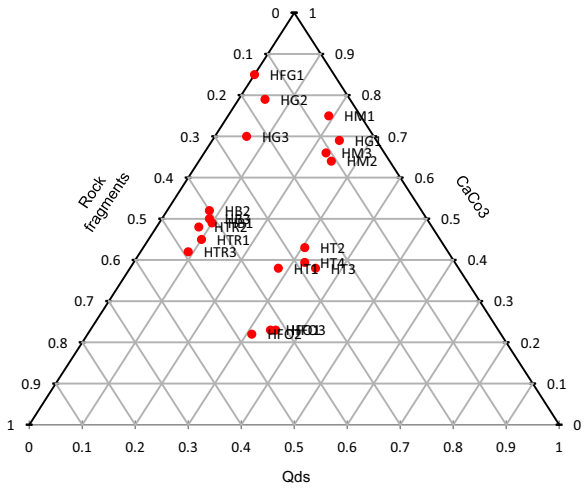

Fig. 11 Ternary diagram, Aggregate compositional distribution (% by volume) of quartz (Qds), Calcite ($CaCO_3$) and Rock fragments (Rf) in the mortars from different sectors of the *Hippo* site

said to be centered-reduced data. And the PCA applied to this transformed data is called normalized PCA [63]. The results of statistical processing by PCA [40] are visualized in the form of two plots. The first plot specific to the method is the loadings plots (circle of correlations in the French-speaking literature), it is visualized in Fig. 12a. It corresponds to a projection of the variables on a two-dimensional plane, made up of two factors (or axes, which accumulate the greatest percentage of variability, axes PC1 and PC2).

Table 9 Main characteristics of mortars groups, the Binder/Aggregate ratio (B/A as wt.% obtained after dissolution of binder)

Group	Colour	Proportion Binder/Aggregate	Sand %	Tile %
M—I	Brownish-white	1:0.5	25	
M—II	Pinkish white	1:1	54	
M—III	Reddish white	1:2	45	< 10
M—IV	Greyish white	1:3	48	< 2

When two variables are far from the centre of the graph, then if they are: (i) close to each other, then they are significantly positively correlated (correlation coefficient r: close to 1); (ii) orthogonal to each other, then they are significantly uncorrelated (r: close to 0); (iii) symmetrically opposite with respect to the centre, then they are significantly negatively correlated (r:close to -1).

Now, when the variables are relatively close to the centre of the loadings plots, then any interpretation is

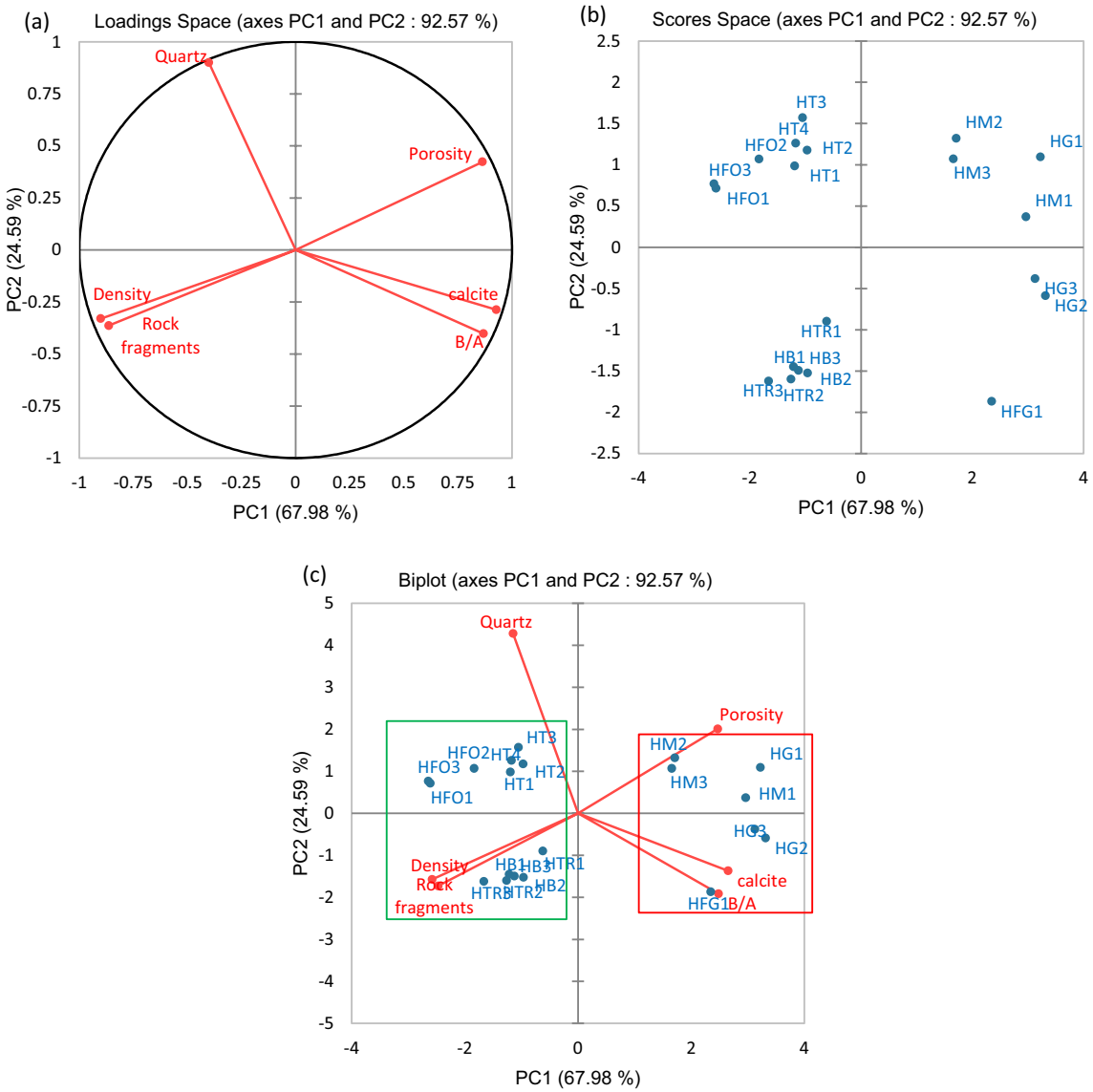

Fig. 12 Loadings **a** and scores **b** of the standardise *Hippo* mortar data; **c** biplot scores and loadings

hazardous, it is therefore necessary to refer to other factorial plans to interpret the results (for example, PC1 and PC3).

In our case study, we note from the loadings plot of Fig. 12a that the variables: density, presence rate of rock fragments, are strongly correlated (or linked). Indeed, when the presence rate of rock fragments increases in a mortar, its density increases and the porosity decreases. The same trend is observed for the calcite content and the binder/aggregate ratio. On the other hand, it is clear that the quartz content and the porosity are independent of each other (or not linked). The loadings plot is also useful for interpreting the meaning of the axes. In our case study, the PC1 axis is clearly linked to the density (and/or the porosity) of the mortar and to the dosage of the binder. While the PC2 axis is essentially linked to the presence of the sand. These trends are particularly interesting to identify for the interpretation of the scores plot (Figs. 12b). The scores plot in Fig. 12b corresponds to one of the objectives of the PCA. It makes it possible to represent the samples on a two-dimensional map, and thus to identify trends. We see in Fig. 12c that the samples which are on the right of the combined scores *vs* loadings plots (Fig. 12c red rectangle), have a porosity and a high B/A ratio, therefore a mortar rich in lime. This is the case here,

Table 10 Quality of the representation of loadings and scores (observations and variables) with respect to PCA axes

	PC1	PC2	PC3	PC4	PC5
Loadings					
Quartz	0.161	**0.811**	0.006	0.022	0.000
Calcit	**0.860**	0.083	0.050	0.007	0.000
Rock fragments	**0.747**	0.132	0.121	0.000	0.000
Porosity	**0.745**	0.179	0.045	0.012	0.018
B/A	**0.753**	0.162	0.009	0.075	0.001
Density	**0.813**	0.109	0.056	0.000	0.022
Scores					
HFO1	**0.891**	0.067	0.001	0.042	0.000
HFO2	**0.580**	0.197	0.222	0.001	0.000
HFO3	**0.877**	0.074	0.000	0.048	0.001
HB1	0.405	**0.574**	0.019	0.000	0.001
HB2	0.278	**0.695**	0.018	0.004	0.005
HB3	0.357	**0.628**	0.015	0.001	0.000
HFG1	**0.554**	0.351	0.081	0.004	0.010
HG1	**0.862**	0.099	0.003	0.035	0.000
HG2	**0.954**	0.030	0.014	0.002	0.000
HG3	**0.848**	0.013	0.135	0.001	0.004
HT1	**0.547**	0.372	0.002	0.074	0.004
HT2	0.350	**0.514**	0.089	0.045	0.002
HT3	0.276	**0.615**	0.017	0.000	0.092
HT4	0.436	**0.502**	0.043	0.009	0.010
HM1	**0.922**	0.014	0.020	0.030	0.014
HM2	**0.584**	0.349	0.024	0.036	0.007
HM3	**0.624**	0.261	0.056	0.050	0.009
HTR1	0.202	**0.420**	0.325	0.051	0.002
HTR2	0.382	**0.612**	0.001	0.002	0.003
HTR3	**0.507**	0.481	0.009	0.001	0.003

The values in bold Correspond, for each variable to the factor (axis) for which the squared cosine is the greatest

of the *market* (HM1–3) and of the *garum* (HG1–3). In contrast, the samples on the left (Fig. 12c green rectangle), are rather dense with a low B/A ratio, therefore a mortar essentially based on rock fragments (gravelly) and also poor in lime. This is the case, for example, of the *Roman theatre* (HTR1-3), the *forum* (HFO1–3) and the *basilica* (HB1–3). Looking at the data on plane F1 and F2 (Fig. 12c), we see that the samples located at the top of the diagram are sandy (quartz, high), while those at the bottom are rather gravelly (fragment rock, high). The quality of representation of the variables on the PCA map (loadings or scores plots) is called cos^2 (square cosine), determined as being, the square of the correlation coefficient of each variable with the axes of the PCA [64]. This can be done by consulting the table of the cos^2 (Table 10). A high cos^2 indicates a good representation of the variable on the main axes under consideration. And a low cos^2 indicates the opposite [64]. It is easy to verify that for each variable or observation, the horizontal sum of the cos^2 (when taking all the components) is equal to 1 (ref). So, we can say that the PC1 and PC2 axes support the majority of the information (or inertia) generated by the PCA (PC1 and PC2: 92.57%).

Scanning electron microscopy was used to search for additional information on the presence of hydraulic compounds. Calcium carbonate should be the only compound of the binder if the limestone is totally pure and no reaction occurs with the aggregate. Here it is clear that other compounds are present. These are the areas marked with the number two (2) of the images in Fig. 13, consisting of calcium, silicon, aluminium, potassium, and magnesium. The analyses performed on the binder by SEM–EDS (HTR Fig. 13a) also highlighted a significant presence of chlorine. This means that all the sampled mortars are probably affected by decay phenomena linked to the presence of sodium chloride. This can be explained by the proximity of *Hippo* to the Mediterranean Sea, which is only a few hundred meters away. In fact, marine aerosols transport sodium chloride in suspension, depositing it on the surface of the architectural structure. These results are in good agreement with the XRPD analysis, where mainly calcite and quartz were observed. In zone 2, an elemental composition of Ca, Al, and Si is detected, which is consistent with the C–A–S–H gel [65, 66]. In the HFO and HG samples, Ca, and the main element which appears with Mg in relatively equivalent quantity, in zone 1 Si with Al have a certain similarity (Fig. 12c, d). This composition is compatible with the grouping results obtained by the Agglomerative Hierarchical Clustering (AHC). Area 1 in Fig. 13e is centred on a tile fragment. Analysis of this zone by the EDS detector (Fig. 13e) shows the presence of quartz and feldspar, both in the tile and in the mortar. The tile is composed of aluminium, potassium, silicon and, to a lesser extent, iron, while the mortar matrix is distinguished by its high calcium content. We are therefore in the presence of hydraulic compounds (C–S–H).

Figure 14 represents the mapping of the chemical elements carried out on the HB2 sample by SEM–EDS, it shows that the mortar of the *basilica* is mainly composed of Ca and Si. We observe that the Ca map is perfectly superimposed on the Mg map, which is distributed in the same areas. This is consistent with the presence of calcite and magnesium, highlighted with XRPD analyses (Fig. 7). As for Si, it is distributed mainly in areas with lower Ca content, so it corresponds to quartz particle distribution.

Based on the various physicochemical and petrographic analyses, we can now propose a unified coding

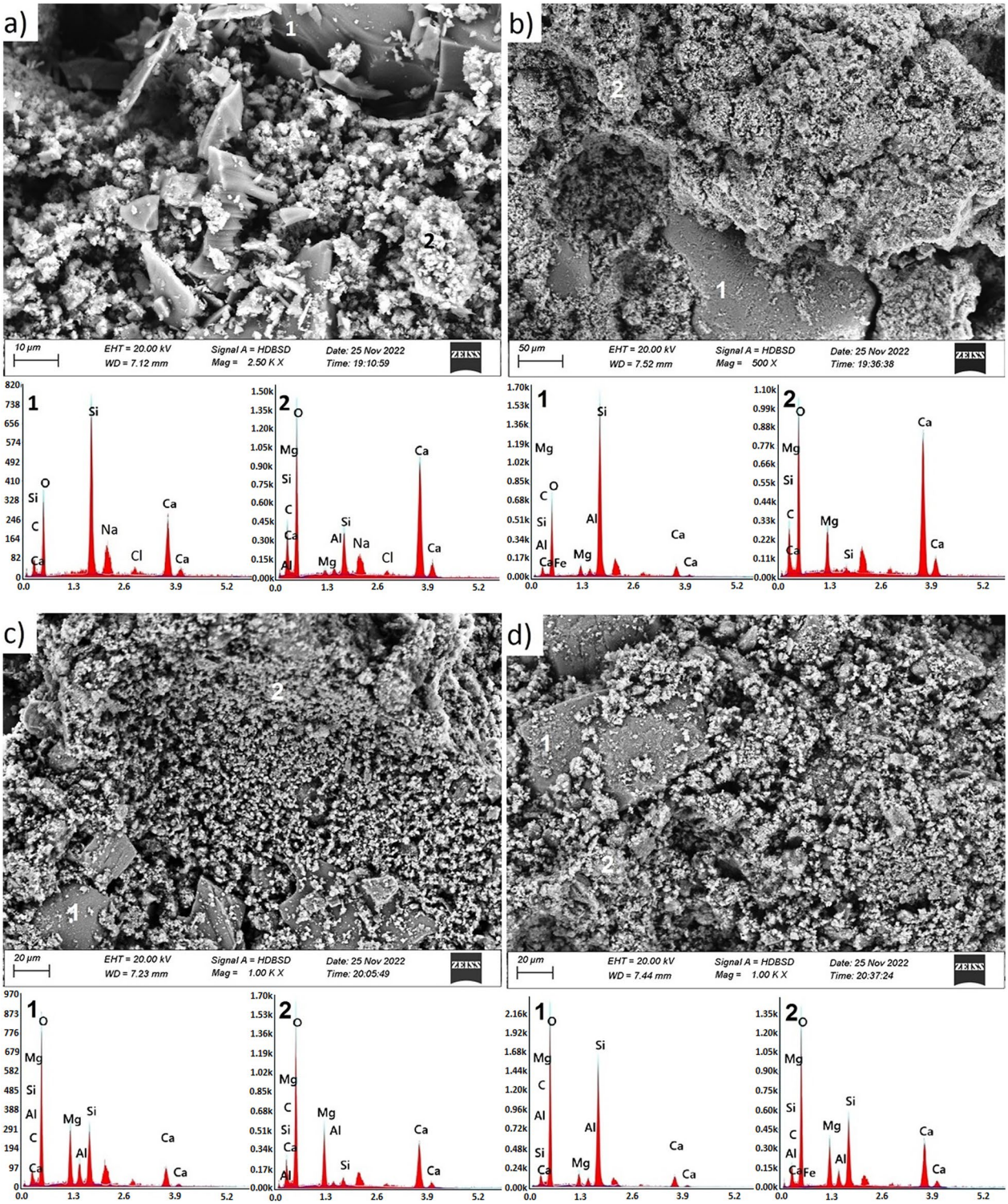

Fig. 13 SEM photographs of various samples. **a** SEM picture from *Roman theatre* sample; **b** SEM picture from *market* sample; **c** SEM picture from *forum* sample; **d** SEM picture from *garum* sample; **e** SEM picture from *Roman baths* sample

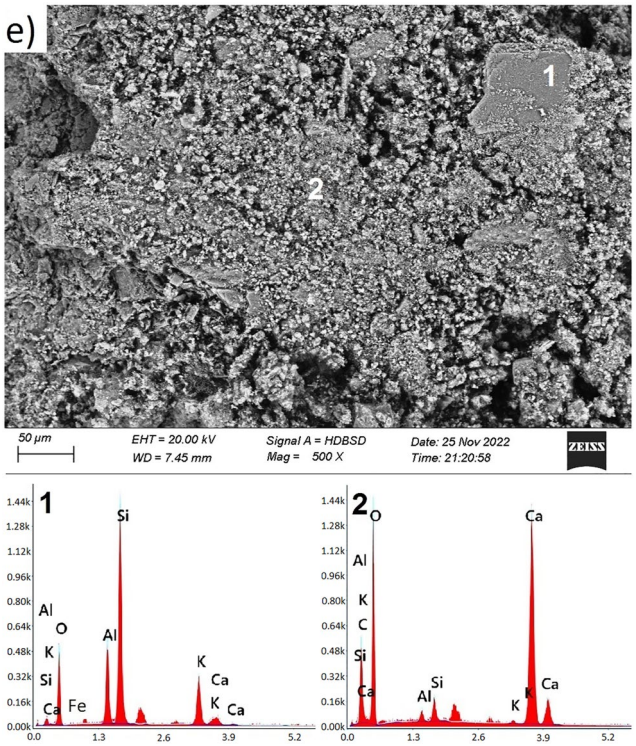

Fig. 13 continued

of the tested samples. This contributes to the identification and final ranking of each sample and consequently each monument. According to Table 11, we find that the crossing of the different groups according to their typological classes (see Sect. Typology of the mortars) and chemical composition (see Sect. Chemical characterization) allowed us to confirm the uniformity and uniqueness of the ingredients and mineralogical components of the materials used in the construction. Indeed, if we are taking as an example the *Roman theatre*, we find that this structure was built in the same chronological interval using a single mortar type.

Conclusion

This work allowed us to trace the general features of the mortar of *Hippo*. Far from being an end in itself, this study proposes a basis for a more global search for the Roman lime mortar present in the various ruins of northeastern Algeria. The application of different analytical techniques (OM, XRF, XRPD, SEM–EDS and TGA), the multivariate statistical approach to the chemical data (cluster analysis) and the principal component analysis from the mineralogical data, combined with previous historic studies, allowed us to achieve the following results:

– The sand used in the lime mortar is mainly based on quartz, probably of marine origin, and rock fragments extracted from the Edough Mountains.

– Statistical analysis by PCA allowed us to quickly extract a wealth of interesting information on the granular nature of the mixture from a set of multidimensional data thanks to two simple graphs: the circle of correlations and the graph of the observations. It appears that, the samples taken from the *garum* (HG1–3) and the *market* (HM1–3) that their mortars are rich in lime and poor in quartz (sand) and rock fragments. And on the contrary, the forum (HFO1–3), has a low rate of calcite (lime) compared to the other monuments. The thermal baths (HT1–4) and the *basilica* (HB1–3) are rather based on gravelly mortar for the *basilica* and sandy for the thermal baths. Consequently, the PCA analysis confirms the conclusions and observation of the typology of mortars and more precisely in terms of the binder/aggregate ratio. The comparison between the historical information and the study of the composition of the mortars of joints allowed us to attribute the HG samples to the first century. Regarding the *Roman baths*, we have succeeded in highlight-

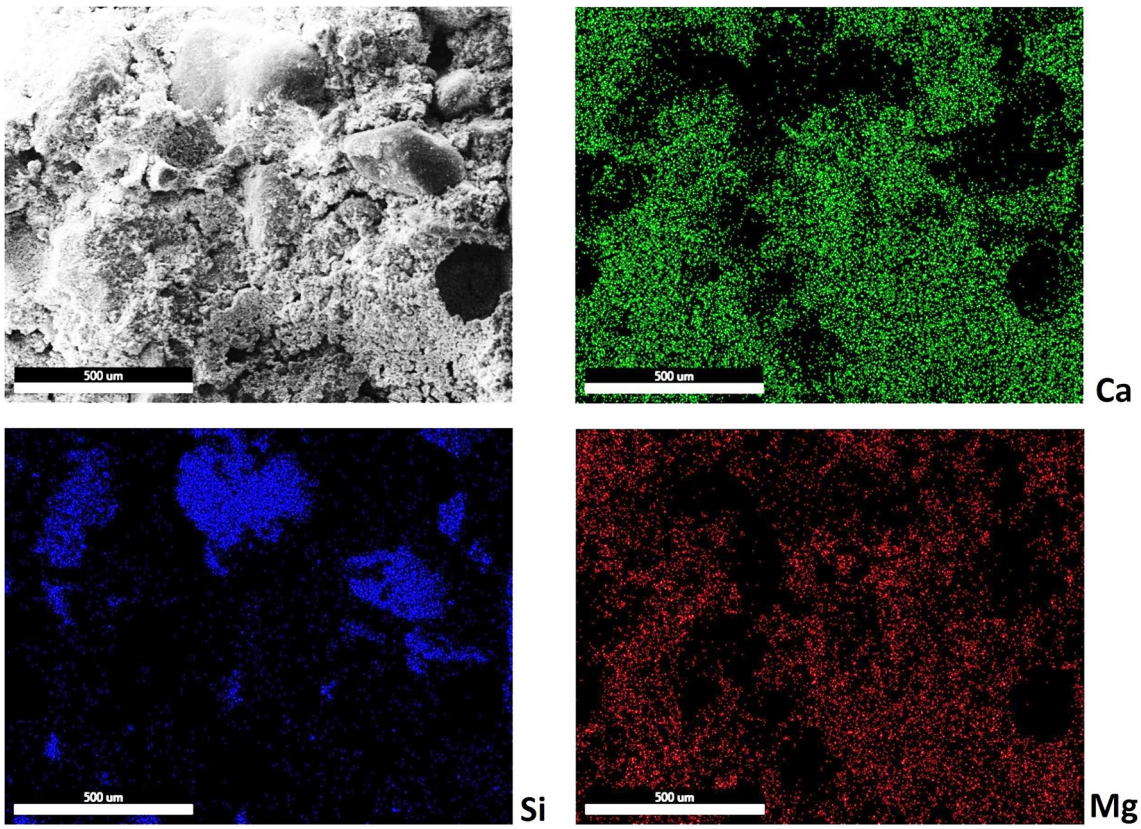

Fig. 14 Micrographs and EDS—mapping of *basilica* simple

ing another type of construction mortar used in old, undocumented rehabilitation or restoration works. For the other monuments, the theoretical dating remains valid and therefore confirmed.

– All binder/aggregate ratios, except for group MI, are less than 1. This means that the aggregate fraction predominates over the binding fraction. This information is very important, as it agrees with the binding/aggregate relationships reported in the technological tradition of Roman construction by Vitruvian in *De Architectura* (Book II, Chapter 5). Indeed, the text of Vitruvian speaks of mortars prepared by mixing two or three parts of aggregate with one part of binder.

– The relatively hydraulic nature of the mixture has been demonstrated, but the origin of this reaction remains to be determined with certainty.

– The low presence of portlandite, visually noted by the absence of calcium hydroxide platelets on SEM imagery, can be explained by the carbonation of the binder phase in contact with atmospheric carbon dioxide. This is due to the high porosity of the cementitious mass of the joint mortars, and to the modern atmospheric pollution of *Hippo* (currently Annaba).

– The presence of kaolinite (a very abundant mineral in the region) suggests the use of broken tiles (the Vitruvian testa). The absence of pozzolan has been proven, showing that the old builders used only local ingredients. Fragment of tiles are also visible from a macroscopic and microscopic point of view, consequently the presence of kaolinite. The detection of this kaolinite, only in the mortar samples taken from the thermal baths, suggests that this presence is not an external contamination by the soil.

Table 11 Final classification and groupage of the lime mortar samples

Sample	Name of monument	Group[a]	Groups controlled by petrographic study and new proposal dating
HFO1	Forum	M—IV—1	1st c
HFO2	Forum	M—IV—1	1st c
HFO3	Forum	M—IV—1	1st c
HB1	Basilica	M—II—2	4–5th c
HB2	Basilica	M—II—2	4–5th c
HB3	Basilica	M—II—2	4–5th c
HFG1	Fountain of the mask of the Gorgon	M—I—1	1st c
HG1	Garum	M—I—1	1st c
HG2	Garum	M—I—1	1st c
HG3	Garum	M—I—1	1st c
HT1	Roman baths	M—III—1	4–5th c
HT2	Roman baths	M—III—2	4–5th c
HT3	Roman baths	M—III—2	4–5th c
HT4	Roman baths	M—III—2	4–5th c
HM1	Roman market	M—I—3	2nd c
HM2	Roman market	M—II—3	2nd c
HM3	Roman market	M—II—3	2nd c
HTR1	Roman theatre	M—II—3	2nd c
HTR2	Roman theatre	M—II—3	2nd c
HTR3	Roman theatre	M—II—3	2nd c

[a] M: Mortar; Roman numeral: attributed groups to the typology presented in paragraph 4.1; Arabic numeral: attributed groups to the typology of chemical composition presented in paragraph Chemical characterization

Abbreviations

γ_r	Real density (g/cm^3)
γ_a	Apparent density (g/cm^3)
N_t	Porosity (%)
M_1	Hydraulic weight of the sample (g)
M_2	Weight of the sample saturated with water (g)
M_S	Weight of the dry sample (g)

Acknowledgements
The sampling was carried out under permission of the Annaba Museum. The author is grateful to Annaba Museum staff for their helpfulness and hospitality, as well as the department of Culture of Annaba city for the granting of all permits necessary to conduct the investigations inside the monuments.

Author contributions
AG: conception development and design of work, analysis, and interpretation of data and drafted the work. All authors read and approved the final manuscript.

Funding
Not applicable.

Availability of data and materials
The datasets used and/or analysed during the current study are available from the corresponding author on reasonable request.

Declarations

Competing interests
The authors declare that they have no competing interests.

Received: 30 August 2022 Accepted: 24 April 2023
Published online: 10 May 2023

References

1. Derdour H. (Annaba, 25 siècles de vie quotidienne et de luttes : menus appendices sur l'histoire générale du Grand Maghreb). (in English. Annaba, 25 centuries of daily life and struggles: appendices menus on the general history of the Great Maghreb). *SNED Editions*. V1. 1982;388.
2. Dahmani S. (Hippone, Hippo regius, collections musées à ciel ouvert). (in English. Hippone, Hippo regius, open-air museums collections). *ARAJA Editions*. 2016;95.
3. Lassus J. Erwan Marec (1888–1968) note biographique). (in English. Erwan Marec (1888–1968), biographical note. Antiq Afr. 1970;4:7–14.
4. Marec E. (Les fouilles d'Hippone). (in English. The excavations of Hippo). Comptes Rendus Des Seances de l'Académie Des Inscriptions et Belles-Lettres. 1948;92(4):558–63.
5. Marec E. (Monuments chrétiens d'Hippone, ville épiscopale de Saint Augustin). (in English. Christian monuments of Hippo, episcopal city of Saint Augustine). Arts et Métiers Graphiques, Paris, France. 1985;260.
6. Barba L, Blancas J, Manzanilla LR, Ortiz A, Barca D, Crisci GM, Miriello D, Pecci A. Provenance of the limestone used in Teotihuacan (Mexico): a methodological approach. Archaeometry. 2009;51:525–45. https://doi.org/10.1111/j.1475-4754.2008.00430.x.
7. Gil E, Mas A, Lerma C, Torner ME, Vercher J. Non-destructive techniques methodologies for the detection of ancient structures under heritage buildings. Int J Archit Heritage. 2019;15(10):1457–73. https://doi.org/10.1080/15583058.2019.1700320.
8. Chiarelli N, Miriello D, Bianchi G, Fichera G, Giamello M, Memmi IT. Characterisation of ancient mortars from the S. Niccolò archaeological complex in Montieri (Tuscany-Italy). Constr Build Mater. 2016;96:442–60. https://doi.org/10.1016/j.conbuildmat.2015.08.023.

9. Moreno-Alcaide M, Compaña-Prieto JM. Roman plasters and mortars from ancient Cosa (Tuscany-Italy). Mineralogical characterisation and construction from domus 10.1 (House with Cryptoporticus). J Archaeol Sci Rep. 2018;19:127–37. https://doi.org/10.1016/j.jasrep.2018.02.025.
10. Dekayir A, Amouric M, Olives J, Parron C, Nadiri A, Chergui A, El Hajraoui MA. Structure et caractérisation des matériaux utilisés dans la construction d'une mosaïque romaine de la cité de Volubilis, Maroc). (in English. Structure and characterization of the materials used in the construction of a Roman mosaic from the city of Volubilis, Morocco. Compt Rendus Geosci. 2004;336:1061–70. https://doi.org/10.1016/j.crte.2004.03.007.
11. De Luca R, Cau Ontiveros MA, Miriello D, Pecci A, Le Pera E, Bloise A, Crisci GM. Archaeometric study o fmortar sand plasters from the Roman City of Pollentia (Mallorca Balearic Islands). Period Mineral. 2013;82(3):353–79. https://doi.org/10.2451/2013PM0021.
12. De Luca R, Gigliotti V, Panarello M, Bloise A, Crisci GM, Miriello D. Spectroscopic, microchemical and petrographic analyses of plasters from ancient buildings in Lamezia Terme (Calabria, Southern Italy). Spectrochim Acta A. 2016;153:184–93. https://doi.org/10.1016/j.saa.2015.08.018.
13. Franzini M, Leoni L, Lezzerini M, Sartori F. The mortar of the "Leaning-Tower" of Pisa: the product of a medieval technique for preparing high-strength mortars. Eur J Mineral. 2000;12:1151–63.
14. Kramar S, Zalar V, Urosevic M, Körner W, Mauko A, Mirtič B, Lux J, Mladenović A. Mineralogical and microstructural studies of mortars from the bath complex of the Roman villa rustica near Mošnje (Slovenia). Mater Char. 2011;62(11):1042–57. https://doi.org/10.1016/j.matchar.2011.07.019.
15. Lezzerini M, Tamponi M, Bertoli M. Calibration of XRF data on silicate rocks using chemicals as in-house standards. Atti Soc Tosc Sci Nat Mem Serie A. 2014;121:65–70.
16. Miriello D, Barca D, Bloise A, Ciarallo A, Crisci GM, De Rose F, Gattuso C, Gazineo F, La Russa MF. Characterisation of archaeological mortars from Pompeii (Campania, Italy) and identification of construction phases by compositional data analysis. J Archaeol Sci. 2010;37(9):2207–23. https://doi.org/10.1016/j.jas.2010.03.019.
17. Miriello D, Barca D, Pecci A, De Luca R, Crisci GM, López Luján L, Barba L. Plasters from different buildings of the sacred precinct of Tenochtitlan (Mexico City): characterization and provenance. Archaeometry. 2015;1:100–27. https://doi.org/10.1111/arcm.12074.
18. Miriello D, Bloise A, Crisci GM, Apollaro C, La Marca A. Characterisation of archaeological mortars and plasters from Kyme (Turkey). J Archaeol Sci. 2011;38:794–804. https://doi.org/10.1016/j.jas.2010.11.002.
19. Riccardi MP, Lezzerini M, Carò F, Franzini M, Messiga B. Micro textural and microchemical studies of hydraulic ancient mortars:two analytical approaches to understand pre-industrial technology processes. J Cult Herit. 2007;8:350–60. https://doi.org/10.1016/j.culher.2007.04.005.
20. Moropoulou A, Bakolas A, Bisbikou K. Investigation of the technology of historic mortars. J Cult Herit. 2000;1(1):45–58. https://doi.org/10.1016/S1296-2074(99)00118-1.
21. Teutonico JM, Ashall G, Garrod E, Yates T. A comparative study of hydraulic lime-based mortars. In BARTOS P., GROOT C. and HUGHES J.J. ed. Historic mortars: characteristics and tests. Proceedings (PRO 12) of the International RILEM Workshop, Paisley (Scotland), 12th-14th May 1999. 2000;339–349.
22. Davidovits F. (Les mortiers de pouzzolanes artificielles chez vitruve evolution et historique architecturale). (in English. Artificial pozzolan mortars in Vitruvian, evolution and architectural history). D.A.S thesis, Universite Paris X, Nanterre, France. 1992.
23. Adam JP. (La construction romaine : matériaux et techniques). (in English. Roman construction: materials and techniques), *Grands manuels Picard*, éditions A. et J. Picard, France. 1995.
24. Perrault C. (Vitruve, Les dix livres d'architecture de Vitruve corrigés et traduits en 1684 par Claude Perrault). (in English.Vitruvian, The ten books of architecture of Vitruvian, corrected and translated in 1684 by Claude Perrault), *Pierre Mardaga éditon*. France. 1979;345.
25. Frizot M. (Le mortier romain mystère ou savoir-faire?) (in English. The Roman mortar, mystery, or know-how?) Dossiers del'archéologie. 1977;25:61–4.
26. Frizot M. (Mortiers et enduits peints antiques, étude technique et archéologique). (in English Ancient painted mortars and coatings, technical and archaeological study), Center for research on Greco-Roman techniques. France: University of Dijon; 1975. p. 351.
27. Miriello D, Barba L, Blancas J, Bloise A, Cappa M, Cura M, De Angelis D, De Luca R, Pecci A, Taranto M, Yavuz BH, Crisci GM. New compositional data on ancient mortars from Hagia Sophia (Istanbul, Turkey). Archaeol Anthropol Sci. 2017;9:499–514. https://doi.org/10.1007/s12520-016-0375-3.
28. Franzini M, Leoni L, Saitta M. Revisione di una metologia analitica per fluorescenza-X, basata sulla correzione completa degli effetti di matric) (in English. Review of an analytical methodology for fluorescence-X, based on the complete correction of matrix effects. Soc It Min Petrol-Rendiconti. 1975;31(2):365–78.
29. Vicat L-J. (Recherches expérimentales sur les chaux de construction, les bétons et les mortiers ordinaires). (in English Experimental research on building limes, concretes and ordinary mortars). *Goujon,* Paris, France. 1818;97.
30. De Luca R, Miriello D, Pecci A, Domínguez-Bella S, Bernal-Casasola D, Cottica D, Bloise A, Crisci GM. Archaeometric study of mortars from the garum shop at pompeii, Campania, Italy. Geoarchaeology. 2015;30:330–51. https://doi.org/10.1002/gea.21515.
31. Armstrong JT. Quantitative elemental analysis of individual microparticles with electron beam instruments. In: Heinrich KFJ, Newbury DE, editors. Electron probe quantitation. New York: Plenum Press; 1991. p. 261–315.
32. Armstrong JT. CITZAF: a package of correction programs for the quantitative electron microbeam X-ray analysis of thick polished materials, thin films, and particles. Microbeam Anal. 1995;4:177–200.
33. NF T46-047. (Caoutchouc et produits en caoutchouc - Détermination de la composition des vulcanisats et des mélanges non vulcanisés par thermogravimétrie). (in English. Rubber and rubber products—determination of the composition of vulcanizates and vulcanized mixtures by thermogravimetry). 2014. Afnor Editions, France.
34. ASTM D5550. Standard test method for specific gravity of soil solids by gas pycnometer. West Conshohocken: ASTM International; 2006.
35. Mota-López MI, Fort R, Álvarez de Buergo M, et al. Characterization of concrete from Roman buildings for public spectacles in *Emerita Augusta* (Mérida, Spain). Archaeol Anthropol Sci. 2018;10:1007–22. https://doi.org/10.1007/s12520-016-0434-9.
36. Mota-López MI, Fort R, Álvarez de Buergo M, et al. Provenance analysis of the granitic ashlars used in the construction of the Roman theatre in *Emerita Augusta* (Merida, Spain). Archaeol Anthropol Sci. 2020;12:236. https://doi.org/10.1007/s12520-020-01192-1.
37. ASTM D6683. Standard test method for measuring bulk density values of powders and other bulk solids as function of compressive stress. West Conshohocken, PA: ASTM International; 2019.
38. AFPC-AFREM. (Détermination de la masse volumique apparente et de la porosité accessible à l'eau). (in English. Determination of bulk density and porosity accessible to water) Report of the technical days. Toulouse, France: K L UNIVERSITY; 1997. p. 121–4.
39. Columbu S, Garau AM, Lugliè C. Geochemical characterisation of pozzolanic obsidian glasses used in the ancient mortars of Nora Roman theatre (Sardinia, Italy): provenance of raw materials and historical–archaeological implications. Archaeol Anthropol Sci. 2019;11:2121–50. https://doi.org/10.1007/s12520-018-0658-y.
40. Lumivero. XLSTAT statistical and data analysis solution. Paris, France. 2022.
41. Uğurlu SE, Hasan ED, Hasan B. Lime mortar technology in ancient eastern Roman provinces. J Archaeol Sci Reports. 2021;39:103132. https://doi.org/10.1016/j.jasrep.2021.103132.
42. Boynton RS. Chemistry and Technology of Lime and Limestone. 2nd ed. New York: Wiley; 1980. p. 592.
43. Miriello D, Lezzerini M, Chiaravalloti F, Bloise A, Apollaro C, Crisci GM. Replicating the chemical composition of the binder for restoration of historic mortars as an optimization problem. Comput Concrete. 2013;12:553–63. https://doi.org/10.12989/cac.2013.12.4.553.
44. Taylor HFW. The chemistry of cements, Volumes 1 and 2. London: Academic Press; 1972.
45. Hadj Zobir S. Impact of weathering on the chemical balance of the diatexites from the Edough Massif (Annaba, NE Algeria). Estudios Geol. 2012;68(2):203–15. https://doi.org/10.3989/egeol.40612.158.
46. Hammor D, Lancelot J. (Métamorphisme miocéne de granites panafricains dans le Massif de l'Edough, Nord-Est de l'Algérie). (in English. Miocene metamorphism of pan-African granites in the Edough Massif, north-eastern of Algeria. Compte Rendus de l'Académie des Sci Paris France série II. 1998;327:391–6.

47. Ahmed Said Y, Leake B-E, Rogers G. The petrology, geochemistry and petrogenesis of the Edough igneous rocks, Annaba, NE Algeria. J Afr Earth Sc. 1993;17(1):111–23. https://doi.org/10.1016/0899-5362(93)90027-N.
48. Gleizes G, Bouleton J, Bossiére G, Collomb P. (Données lithologiques et pétrostructurales nouvelles sur le Massif cristallophyllien de l'Edough, Est Algérien). (in English. New lithological and petrostructural data on the crystallophyllian Massif of Edough, eastern Algeria). Compte Rendus de l'Académie des Sci Paris France series II. 1988;306:1001–8.
49. Hilly J. (Etude géologique du massif de l'Edough et du Cap de Fer, Est constantinois). (in English. Geological study of the Edough massif and Cap de Fer, eastern Constantine). Publications du service de la Carte géologique de l'Algérie (nouvelle série) 19,408. 1962.
50. Bakolas A, Biscontin G, Contardi V, Franceschi E, Moropoulou A, Palazzi D, Zendri E. Thermoanalytical research on traditional mortars in Venice. Thermochim Acta. 1995;269–270:817–28. https://doi.org/10.1016/0040-6031(95)02574-X.
51. Corti C, Rampazzi L, Bugini R, Sansonetti A, Biraghi M, Castelletti L, Nobile I, Orsenigo C. Thermal analysis and archaeological chronology : the ancient mortars of the site of Baradello (Como, Italy). Thermochim Acta. 2013;572:71–84. https://doi.org/10.1016/j.tca.2013.08.015.
52. Marcelo L, de Oliveira G, de Oliveira Freire FL, Ribeiro FRC, Sousa INL, Mesquita E, Bertini AA. Investigation of the mortars and clay bricks of a luso-brazilian historic structure from XVIII century: The Nosso Senhor do Bonfim Church. J Build Eng. 2022;45:103592. https://doi.org/10.1016/j.jobe.2021.103592.
53. Maravelaki-Kalaitzaki P, Bakolas A, Moropoulou A. Physico-chemical study of Cretan ancient mortars. Cem Concr Res. 2003;33(5):651–61. https://doi.org/10.1016/S0008-8846(02)01030-X.
54. Moropoulou A, Bakolas A, Bisbikou K. Physico-chemical adhesion and cohesion bonds in joint mortars imparting durability to the historic structures. Constr Build Mater. 2000;14(1):35–46. https://doi.org/10.1016/S0950-0618(99)00045-8.
55. Genestar C, Pons C, Mas A. Analytical characterisation of ancient mortars from the archaeological Roman city of Pollentia (Balearic Islands, Spain). Anal Chim Acta. 2006;557(1–2):373–9. https://doi.org/10.1016/j.aca.2005.10.058.
56. Ergenç D, Gonzalezv RF. Preliminary investigation of the preparation of repair mortars for the Temple Of Diana, M´erida Spain. Ge-Conservacion. 2017;1(11):42–9. https://doi.org/10.37558/gec.v11i0.443.
57. Bonazza A, et al. Characterization of hydraulic mortars from archaeological complexes in Petra Period. di Mineral. 2013;82(3):459–75. https://doi.org/10.2451/2013PM0027.
58. Paloma P, Santiago M-C, Alfredo I, Laetitia B, Ivan G-J. Pore structure and interdisciplinary analyses in Roman mortars: Building techniques and durability factors identification. Constr Build Mater. 2022;317:12582. https://doi.org/10.1016/j.conbuildmat.2021.125821.
59. Taylor HFW. Cement chemistry. 2nd ed. London: Thomas Telford Publishing; 1997. p. 113–28.
60. Brereton RG. Principal components analysis with several objects and variables. J Chemometrics. 2022. https://doi.org/10.1002/cem.3408.
61. Brereton RG. Graphical introduction to principal components analysis. J Chemometrics. 2022;36:e3404. https://doi.org/10.1002/cem.3404.
62. Bro R, Smilde AK. Centering and scaling in component analysis. J Chemometrics. 2003;17:16–33. https://doi.org/10.1002/cem.773.
63. Bro R, Smilde AK. Principal component analysis. J Anal Methods. 2014;6(9):2812–31. https://doi.org/10.1039/C3AY41907J.
64. F Husson, S Li, J Pagés. (Analyse des données avec R). (in English. Data analysis with R). Presses Universitaires de Rennes. ISBN 978-2-7535-0938-2. 200;224.
65. Pavía S, Caro S. An investigation of Roman mortar technology through the petrographic analysis of archaeological material. Constr Build Mater. 2008;22(8):1807–11. https://doi.org/10.1016/j.conbuildmat.2007.05.003.
66. Rispoli C, Graziano SF, Di Benedetto C, De Bonis A, Guarino V, Esposito R, Morra V, Cappelletti P. New insights of historical mortars beyond pompei: The example of Villa del Pezzolom Sorrento Peninsula. Minerals. 2019;9(10):575. https://doi.org/10.3390/min9100575.

Publisher's Note